

KrkNLO matching for colour-singlet processes

Pratixan Sarmah,^a Andrzej Siódsmok,^a James Whitehead^{a,b}

^a*Jagiellonian University,*

ul. prof. Stanisława Łojasiewicza 11, 30-348 Kraków, Poland

^b*Institute of Nuclear Physics, Polish Academy of Sciences,*

ul. Radzikowskiego 152, 31-342 Kraków, Poland

E-mail: pratixan.sarmah@doctoral.uj.edu.pl, andrzej.siodmok@uj.edu.pl,
james.whitehead@uj.edu.pl

ABSTRACT: Matched calculations combining perturbative QCD with parton showers are an indispensable tool for LHC physics. Two methods for NLO matching are in widespread use: MC@NLO and POWHEG. We describe an alternative, KrkNLO, reformulated to be easily applicable to any colour-singlet process. The primary distinguishing characteristic of KrkNLO is its use of an alternative factorisation scheme, the ‘Krk’ scheme, to achieve NLO accuracy. We describe the general implementation of KrkNLO in Herwig 7, using diphoton production as a test process. We systematically compare its predictions to those produced by MC@NLO with several different choices of shower scale, both truncated to one-emission and with the shower running to completion, and to ATLAS data from LHC Run 2.

KEYWORDS: QCD, LHC, NLO matching, parton showers, factorisation schemes, hadron colliders

Contents

1	Introduction	1
2	NLO matching with KrkNLO	2
2.1	Notation and definitions	2
2.2	The KrkNLO method	10
2.3	The Krk factorisation scheme	12
2.4	Comparison with MC@NLO	14
3	Implementation	15
3.1	KrkNLO in Herwig 7	16
3.2	Validation	16
3.2.1	Real matrix elements	16
3.2.2	Virtual matrix elements	17
3.2.3	Krk factorisation scheme	17
4	Analysis of NLO matching uncertainty	18
4.1	First-emission only	20
4.2	Full shower	20
5	Results and phenomenology	26
6	Conclusion	28
A	Summary of Catani–Seymour insertion operators	29
B	PDFs in the Krk factorisation scheme	31
C	Validation	33

1 Introduction

In the precision era of LHC physics, ‘matched’ calculations combining next-to-leading-order (NLO) perturbative accuracy with the all-orders logarithmic resummation provided by parton shower algorithms remain an indispensable workhorse for LHC phenomenology. Two methods for matching at NLO, the MC@NLO [1] and POWHEG methods [2–4], have been widely used for LHC physics and the associated matching uncertainties investigated in detail for a wide variety of processes and for a number of independent implementations in [5–17].

The differences between results generated by alternative matching schemes may be considered ‘matching uncertainties’, the full general extent of which is unclear, but which comprise formally higher-order terms introduced beyond NLO by the choice of matching method.

In order to achieve the goal of a fully-general matching method to combine parton showers with NNLO fixed-order calculations, it is necessary to look beyond established matching methods to alternatives which may more readily admit generalisation beyond NLO. Early efforts in the direction of general NNLO matching include NNLOPS [18], UN²LOPS and similar [19–22], GENEVA [23–25] and MiNNLO_{PS} [26]. Simultaneously, exploring alternative schemes at NLO allows a better

assessment of the magnitude and significance of matching uncertainties for matched NLO+PS predictions.

The KrkNLO method for parton shower matching [27–29] is one such alternative. Its key feature is to exploit the general freedom (at NLO and beyond) to choose a PDF factorisation scheme for the calculation. The factorisation scheme employed (the ‘Krk scheme’ [30]) is defined by the requirement that it remove the double-counting between real- and shower-emissions which lies at the heart of the NLO matching problem.

The KrkNLO method has previously been formulated and implemented for a simplified version of the Drell-Yan process [28] and for Higgs production via gluon fusion in the infinite-top-mass limit [29].

In this work, we refresh and extend the formulation to the production of arbitrary colour-singlet final-states which proceed via $q\bar{q}$ -annihilation at leading-order. As an initial test process to study matching uncertainty we consider diphoton production, where the absence of a resonance peak and the characteristic falling spectrum offer a useful sandbox for the identification of different contributions.

This is the first process calculated independently of the derivation of the Krk factorisation scheme and is an intermediate step towards a fully-automated calculation for arbitrary colour-singlet final-states, which will be the subject of a future publication.

In section 2 we introduce and re-formulate the KrkNLO method, alongside the MC@NLO method in comparable notation; in section 3 we describe its implementation in Herwig 7.

Interested readers who wish to bypass the technicalities of section 2 on first reading may prefer to begin with sections 4 and 5. In section 4 we compare the method with the MC@NLO method, both after a single emission and after the parton shower has been allowed to run to its conclusion. In section 5 we compare the alternative methods with LHC Run II data from ATLAS.

2 NLO matching with KrkNLO

The KrkNLO method was introduced in [28, 29] following preliminary work in [27, 31]; the Krk factorisation scheme, which will be introduced below, was the subject of dedicated discussion in [30, 32].

In section 2.1 we establish notation for NLO fixed-order calculations, parton showers, and NLO matching and review the MC@NLO method in this notation. In section 2.2 we outline the KrkNLO method for a general process $pp \rightarrow X$ with no QCD partons in the final state. In section 2.3 we motivate and summarise the necessary factorisation scheme transformation into the Krk scheme for the NLO matching condition to be satisfied. Finally in section 2.4 we summarise the difference in higher-order terms between KrkNLO and MC@NLO that can be expected to contribute to the differences observed in practice in section 4.

2.1 Notation and definitions

QCD at NLO

We write the differential hadronic cross-section for $2 \rightarrow m$ process $A + B \rightarrow X$, for an (IRC-safe) observable’s measurement function \mathcal{O} , within the framework of collinear factorisation as

$$d\sigma_{AB}[\mathcal{O}](P_1, P_2) = d\xi_1 d\xi_2 \sum_{a,b} f_a^A(\xi_1, \mu_F) f_b^B(\xi_2, \mu_F) d\hat{\sigma}_{ab}[\mathcal{O}](\xi_1 P_1, \xi_2 P_2) \quad (2.1)$$

for partonic flavours a, b , $\overline{\text{MS}}$ parton distribution functions f_a^A, f_b^B , incoming hadronic momenta P_1, P_2 and collinear momentum fractions $\xi_{1,2}$, and where implicitly we further allow the factorisation

scale μ_F to be an infrared-safe function of the phase-space kinematics. The partonic differential cross-section may be expanded perturbatively to next-to-leading-order,

$$d\hat{\sigma}_{ab}[\mathcal{O}](\xi_1 P_1, \xi_2 P_2) = \left(\frac{\alpha_s(\mu_R)}{2\pi} \right)^k \left[d\hat{\sigma}_{ab}^{(0)}[\mathcal{O}](\xi_1 P_1, \xi_2 P_2) + \left(\frac{\alpha_s(\mu_R)}{2\pi} \right) d\hat{\sigma}_{ab}^{(1)}[\mathcal{O}](\xi_1 P_1, \xi_2 P_2; \mu_F, \mu_R) + \mathcal{O}(\alpha_s^2) \right], \quad (2.2)$$

where μ_R is the renormalisation scale and for the processes we consider subsequently, $k = 0$.

The leading-order contribution $d\hat{\sigma}_{ab}^{(0)}$ is given by

$$d\hat{\sigma}_{ab}^{(0)}[\mathcal{O}](\xi_1 P_1, \xi_2 P_2) = d\Phi_m(\xi_1 P_1, \xi_2 P_2) \frac{1}{2\hat{s}_{12}} B_{ab}(\Phi_m) \Theta_{\text{cut}}[\Phi_m] \mathcal{O}(\Phi_m) \quad (2.3)$$

where $d\Phi_m$ denotes the m -particle (Born) Lorentz-invariant phase-space measure, B_{ab} the Born matrix-element for the partonic channel ab , and $\Theta_{\text{cut}}[\Phi_m]$ a theta-function imposing ‘generator’ cuts on the Born phase-space; fiducial cuts where different are included within the definition of \mathcal{O} .¹ The partonic flux factor $1/(2\hat{s}_{12})$ contains the momentum invariant between the incoming partons,

$$\hat{s}_{12} = (p_1 + p_2)^2 = 2p_1 \cdot p_2 \quad (2.4)$$

For brevity we suppress the arguments of $d\Phi_m$ where unambiguous.

The next-to-leading-order (NLO) contribution may be written using the subtraction formalism as

$$\begin{aligned} d\hat{\sigma}_{ab}^{(1)}[\mathcal{O}](\xi_1 P_1, \xi_2 P_2) &= d\Phi_m \frac{1}{2\hat{s}_{12}} \left[V_{ab}(\Phi_m) + \sum_{(\alpha)} B_{ab}^{(\alpha)}(\Phi_m) \int d\Phi_{+1}^{(\alpha)} x S^{(\alpha)}(\Phi_{+1}^{(\alpha)}) \right] \Theta_{\text{cut}}[\Phi_m] \mathcal{O}(\Phi_m) \\ &+ d\eta_1 d\eta_2 d\Phi_m(\eta_1 \xi_1 P_1, \eta_2 \xi_2 P_2) \frac{1}{2\hat{s}_{12}} C_{ab}^{\text{FS}}(\eta_1, \eta_2; \mu_F; \Phi_m) \Theta_{\text{cut}}[\Phi_m] \mathcal{O}(\Phi_m) \\ &+ d\Phi_{m+1} \frac{1}{2\hat{s}_{12}} \left[R_{ab}(\Phi_{m+1}) \Theta_{\text{cut}}[\Phi_{m+1}] \mathcal{O}(\Phi_{m+1}) \right. \\ &\quad \left. - \sum_{(\alpha)} S^{(\alpha)}(\tilde{\Phi}_{+1}^{(\alpha)}) B^{(\alpha)}(\tilde{\Phi}_m^{(\alpha)}) \Theta_{\text{cut}}[\tilde{\Phi}_m^{(\alpha)}] \mathcal{O}(\tilde{\Phi}_m^{(\alpha)}) \right], \end{aligned} \quad (2.5)$$

for virtual matrix-elements V , real matrix-elements R , mass-factorisation counterterms C^{FS} , subtraction kernels $S^{(\alpha)}$ with corresponding phase-space mappings $\tilde{\Phi}_m^{(\alpha)}(\Phi_{m+1})$ and $\tilde{\Phi}_{+1}^{(\alpha)}(\Phi_{m+1})$ and reduced matrix-elements $B^{(\alpha)}$, all indexed by generalised index (α) . We suppress an implicit summation over colour- and spin-indices between the subtraction kernels $S^{(\alpha)}$ and the corresponding reduced-matrix-elements $B^{(\alpha)}$.

Here we adopt the momentum mappings and subtraction terms of Catani–Seymour dipole subtraction [33]. For our purposes, initial-initial dipoles suffice, so we employ the notation²

$$\left. \begin{array}{l} p_1 = \xi_1 P_1 \quad \text{emitter} \\ p_2 = \xi_2 P_2 \quad \text{spectator} \\ q \quad \text{emission} \\ \{q_i\}_{i=1}^m \quad \text{FS particles} \end{array} \right\} = \Phi_{m+1}(p_1, p_2) \mapsto \tilde{\Phi}_m^{\text{II}_1}(\Phi_{m+1}) = \begin{cases} p_1^{\text{II}_1} = x p_1 = x \xi_1 P_1 \\ p_2^{\text{II}_1} = p_2 = \xi_2 P_2 \\ q_i^{\text{II}_1} = \Lambda(p_1 + p_2 - q, p_1^{\text{II}_1} + p_2^{\text{II}_1}) q_i \end{cases} \quad (2.6)$$

¹In particular, where the Born phase-space contains limits in which the Born matrix-element diverges, Θ_{cut} must be chosen to remove them by, at the very least, imposing a technical cut vetoing the singular regions.

²The corresponding mapping in which the second incoming parton is the emitter, II_2 , may be obtained by relabelling.

where

$$x = x^{\text{II}_1}(\Phi_{m+1}) = 1 - \frac{q \cdot (p_1 + p_2)}{p_1 \cdot p_2} \equiv x^{\text{II}_2}(\Phi_{m+1}) \quad (2.7)$$

is the collinear momentum fraction of the splitting and Λ a Lorentz transformation restoring over-all momentum conservation by mapping $p_1 + p_2 - q$ onto $p_1^{\text{II}_1} + p_2^{\text{II}_1}$. We require only $(\alpha) \in \{(q_a g_i, b), (g_a q_i, b)\}$ in the notation of [33], with

$$S^{(\alpha)}(x) = \frac{8\pi}{x s_{ai}} D^{(\alpha)}(x) \quad (2.8)$$

where the momentum invariant s_{ai} is between the emitter and the emission, and

$$D^{(q_a g_i, b)}(x) = C_F \frac{1+x^2}{1-x} \quad D^{(g_a q_i, b)}(x) = T_R (x^2 + (1-x)^2). \quad (2.9)$$

We omit the spectator from the label (α) where unambiguous. We further write the integrated dipoles

$$B^{(\alpha)}(\Phi_m) \int d\Phi_{+1}^{(\alpha)} x S^{(\alpha)}(\Phi_{+1}^{(\alpha)}) \quad (2.10)$$

as the sum of a fully-integrated part in the Born phase-space $I^{(\alpha)}(\Phi_m)$ and a collinear contribution which we write schematically as $K^{(\alpha)}(x) B^{(\alpha)}(\Phi_m)$ and combine with the mass-factorisation counterterms C , which comprise the DGLAP splitting kernels.

For colour-singlet final-states, we may write the simplified expression for each $q\bar{q}$ channel as

$$\begin{aligned} d\hat{\sigma}_{q\bar{q}}^{(1)}[\mathcal{O}](\xi_1 P_1, \xi_2 P_2) &= d\Phi_m \frac{1}{2\hat{s}_{12}} \left[V_{q\bar{q}}(\Phi_m) + I_{q\bar{q}}(\Phi_m) \right] \mathcal{O}(\Phi_m) \\ &+ d\eta_1 d\eta_2 d\Phi_m(\eta_1 \xi_1 P_1, \eta_2 \xi_2 P_2) \frac{1}{2\hat{s}_{12}} \left[(P(\mu_F) + K^{\text{FS}})_{q\bar{q}}(\eta_1) B_{q\bar{q}}(\Phi_m) \delta_{\eta_2}^1 \right. \\ &\quad \left. + \delta_{\eta_1}^1 B_{q\bar{q}}(\Phi_m) (P(\mu_F) + K^{\text{FS}})_{q\bar{q}}(\eta_2) \right] \mathcal{O}(\Phi_m) \\ &+ d\Phi_{m+1} \frac{1}{2\hat{s}_{12}} \left[R_{q\bar{q}}(\Phi_{m+1}) \mathcal{O}(\Phi_{m+1}) \right. \\ &\quad \left. - \frac{8\pi}{x} D^{(qg)}(x) \left[\frac{1}{s_{qg}} B_{q\bar{q}}(\tilde{\Phi}_m^{\text{II}_1}) \mathcal{O}(\tilde{\Phi}_m^{\text{II}_1}) + \frac{1}{s_{\bar{q}g}} B_{q\bar{q}}(\tilde{\Phi}_m^{\text{II}_2}) \mathcal{O}(\tilde{\Phi}_m^{\text{II}_2}) \right] \right], \end{aligned} \quad (2.11)$$

dropping the Θ_{cut} factors for brevity, and writing $\delta_{\eta_i}^1$ as a shorthand for the Dirac delta function $\delta(1 - \eta_i)$. Explicit expressions for the P and K contributions are given in appendix A. Likewise for each qg -type channel,

$$\begin{aligned} d\hat{\sigma}_{qg}^{(1)}[\mathcal{O}](\xi_1 P_1, \xi_2 P_2) &= d\eta_1 d\eta_2 d\Phi_m(\eta_1 \xi_1 P_1, \eta_2 \xi_2 P_2) \frac{1}{2\hat{s}_{12}} \delta_{\eta_1}^1 B_{q\bar{q}}(\Phi_m) (P(\mu_F) + K^{\text{FS}})_{gq}(\eta_2) \mathcal{O}(\Phi_m) \\ &+ d\Phi_{m+1} \frac{1}{2\hat{s}_{12}} \left[R_{qg}(\Phi_{m+1}) \mathcal{O}(\Phi_{m+1}) - S^{(gq)}(x) B_{q\bar{q}}(\tilde{\Phi}_m^{\text{II}_2}) \mathcal{O}(\tilde{\Phi}_m^{\text{II}_2}) \right], \end{aligned} \quad (2.12)$$

and similarly for $d\hat{\sigma}_{g\bar{q}}^{(1)}$.

Parton showers

A parton shower typically uses the veto algorithm [34–38] to sample successive splitting scales from the so-called Sudakov distribution characterising the probability of generating a splitting of type i at a scale $t \in (t_0, t_1)$,

$$p_i(t; t_0, t_1) = \Theta[t_0 < t < t_1] P_i(t) \Delta_t^{\left| t_1 \right.}, \quad (2.13)$$

where $P_i(t)$ represents the conditional probability density that a splitting of type i occurs at scale t given that no splitting has occurred at a higher scale, and

$$\Delta|_t^{t_1} = \prod_i \Delta_i|_t^{t_1} \quad (2.14)$$

represents the Sudakov factor describing the ‘survival’ probability that no splitting is generated between scales t and t_1 , i.e. concretely

$$p_\emptyset(t; t_0, t_1) = \delta(t - 0) \Delta|_{t_0}^{t_1}. \quad (2.15)$$

Solving the resulting differential equations,

$$\frac{d}{dt} \Delta_i|_t^{t_1} = \Delta_i|_t^{t_1} P_i(t), \quad (2.16)$$

for a single splitting, and

$$\frac{d}{dt} \Delta|_t^{t_1} = \sum_i p_i(t; t_0, t_1) = \Delta|_t^{t_1} \sum_i P_i(t), \quad (2.17)$$

for all splittings, in the possible-splitting region, gives the closed-form expressions for the Sudakov factor associated with each splitting,

$$\Delta_i|_t^{t_1} = \exp \left[- \int_t^{t_1} dt' P_i(t') \right], \quad (2.18)$$

and that associated with all splittings,

$$\Delta|_t^{t_1} = \prod_i \Delta_i|_t^{t_1} = \exp \left[- \int_t^{t_1} dt' \sum_i P_i(t') \right]. \quad (2.19)$$

For each scale sampled from this distribution the shower generates a higher-multiplicity phase-space configuration in which an additional resolved emission has the generated scale, with kinematics distributed in phase-space according to some kernel related to the density by

$$P_i(t) = \int d\Phi_{+1} \frac{\alpha_s(\mu(\Phi_{+1}))}{2\pi} P_i(\Phi_{+1}) \delta(t - t(\Phi_{+1})). \quad (2.20)$$

In practice, the possible splittings and splitting phase-space available to be considered for each splitting depend further on the initial phase-space configuration, allowing us to express the action of the parton shower formally as an iterative operator,

$$\text{PS}[\mathcal{O}](\Phi_m; \boldsymbol{\xi}) = \Delta|_{t_0}^{t_1(\Phi_m)}(\Phi_m; \boldsymbol{\xi}) \mathcal{O}(\Phi_m) \quad (2.21)$$

$$\begin{aligned} &+ \sum_{(\alpha) \in \Phi_m} d\Phi_{+1}^{(\alpha)} \Theta \left[t_0 < t(\Phi_{+1}^{(\alpha)}) < t_1(\Phi_m) \right] \left(\frac{\alpha_s(\mu^{(\alpha)}(\Phi_{+1}^{(\alpha)}))}{2\pi} P_m^{(\alpha)}(\Phi_{+1}^{(\alpha)}; \boldsymbol{\xi}) \right) \\ &\times \Delta|_{t(\Phi_{+1}^{(\alpha)})}^{t_1(\Phi_m)}(\Phi_m; \boldsymbol{\xi}) \text{PS}[\mathcal{O}](\Phi_{+1}^{(\alpha)}; \boldsymbol{\xi}^{(\alpha)}), \end{aligned} \quad (2.22)$$

where we replace index i with a generalised index (α) to represent the possible splittings from momentum configuration Φ_m , m to indicate the final-state multiplicity, and $\boldsymbol{\xi} = (\xi_1, \xi_2)$ denotes the incoming partonic momentum-fractions. For brevity we will write

$$\Theta_{t_0}^{t_1(\Phi_m)} \equiv \Theta \left[t_0 < t(\Phi_{+1}) < t_1(\Phi_m) \right] \quad (2.23)$$

when the argument of the Θ -function is unambiguous. Assembling the components, the Sudakov factor $\Delta|_{t_0}^{t_1(\Phi_m)}(\Phi_m; \boldsymbol{\xi})$ may be expanded perturbatively as

$$\Delta|_{t_0}^{t_1(\Phi_m)}(\Phi_m; \boldsymbol{\xi}) \equiv \prod_{(\alpha) \in \Phi_m} \Delta_{(\alpha)}|_{t_0}^{t_1(\Phi_m)}(\Phi_m; \boldsymbol{\xi}) \quad (2.24)$$

$$= 1 - \frac{\alpha_s}{2\pi} \sum_{(\alpha) \in \Phi_m} \int d\Phi_{+1}^{(\alpha)} \Theta_{t_0}^{t_1(\Phi_m)} P_m^{(\alpha)}(\Phi_{+1}^{(\alpha)}; \boldsymbol{\xi}^{(\alpha)}) + O(\alpha_s^2). \quad (2.25)$$

For brevity one or both of the phase-space and partonic momentum-fraction arguments of Δ will typically be omitted where unambiguous. In full generality the cut-off t_0 may be a function of the underlying phase-space, $t_0(\Phi_m)$; here we restrict to the case where it is a constant.³

The PS operator acts as a functional on the measurement function of IRC-safe observable \mathcal{O} and represents a single iteration of the shower algorithm: either a splitting is selected and performed (the second term), or no resolvable emission is generated above the cut-off scale, in which case the observable is evaluated on the input phase-space configuration and the iteration is terminated (the first term).

The case when \mathcal{O} consists only of a product of theta-functions and $\mathcal{O}(\Phi_m) \equiv \mathcal{O}(\Phi_n)$ for all $n \geq m$ corresponds to a calculation of the inclusive cross-section, by unitarity, ‘integrating out’ all possible shower emissions. Unitarity can be verified at NLO by comparing the first-order expansion of the Sudakov factor eq. (2.25) to the corresponding differential contributions in eq. (2.21).

The choices of $t(\Phi_m)$, $P_m^{(\alpha)}$ and $\Phi_{+1}^{(\alpha)}$ define the parton shower algorithm. We will focus upon the (Catani–Seymour) dipole shower [39–43] and concretely, its implementation in Herwig 7 [9, 44, 45], in which the ordering variable t is the transverse momentum of the emitted parton relative to the emitter-spectator pair in its rest-frame, the splitting densities $P_m^{(\alpha)}$ are chosen to be Catani–Seymour dipole functions [33, 46], and the phase-space factorisation implicit in eq. (2.21) is provided by the corresponding Catani–Seymour momentum mappings.

The dipole functions relevant to the NLO matching of processes considered in the present work are the same polarisation-averaged initial–initial splitting dipoles used for dipole subtraction in eq. (2.9) [42]. The initial–initial massless momentum mapping is given, without loss of generality labelling p_1 as the emitter, by

$$\left. \begin{array}{l} p_1 = \xi_1 P_1 \quad \text{emitter} \\ p_2 = \xi_2 P_2 \quad \text{spectator} \\ \{q_i\}_{i=1}^m \quad \text{FS} \end{array} \right\} = \Phi_m(p_1, p_2) \xrightarrow{\Phi_{+1}} \Phi_{m+1}^{\text{II}_1} = \begin{cases} p_1^{\text{II}_1} = x^{-1} p_1 = x^{-1} \xi_1 P_1 \\ p_2^{\text{II}_1} = p_2 = \xi_2 P_2 \\ q_i^{\text{II}_1} = \Lambda(p_1 + p_2, p_1^{\text{II}_1} + p_2^{\text{II}_1} - q_{m+1}^{\text{II}_1}) q_i \\ q_{m+1}^{\text{II}_1} = (1 - x - v) p_1^{\text{II}_1} + v p_2 + k_{\text{T}} \end{cases} \quad (2.26)$$

where Λ is a Lorentz transformation restoring overall momentum conservation. This is the inverse mapping of eq. (2.6) and we will implicitly use that

$$\tilde{\Phi}_m^{(\alpha)}(\Phi_{m+1}^{(\alpha)}(\Phi_m, \Phi_{+1})) = \Phi_m, \quad \tilde{\Phi}_{+1}^{(\alpha)}(\Phi_{m+1}^{(\alpha)}(\Phi_m, \Phi_{+1})) = \Phi_{+1}, \quad (2.27)$$

and $x(\Phi_{m+1}^{(\alpha)}(\Phi_m, \Phi_{+1})) = x$.

The transverse momentum of the generated splitting in eq. (2.26) is governed by k_{T} , a massless four-vector generated with uniformly-distributed azimuth around the emitter-spectator axis in the rest frame of the emitter-spectator pair, with spatial magnitude given by

$$\|\mathbf{k}_{\text{T}}\|^2 = \frac{1}{x} v (1 - x - v) \hat{s}_{12}. \quad (2.28)$$

³In this context, the shower cut-off is typically tuned alongside hadronisation model parameters to give good agreement with data. Although we will not discuss hadronisation, this fixed shower cut-off is in practice used as a scale governing the transition from the parton shower model to the non-perturbative hadronisation model.

We will denote the transverse momentum of the i^{th} generated splitting, with respect to its emitter-spectator pair in the dipole rest frame, as $p_{T,i}$.

The three random variables which parametrise the three additional dimensions required to describe an $(m+1)$ -particle phase-space from an m -particle phase-space are therefore x, v and ϕ , and give rise to a convolution over the collinear momentum fraction x ,

$$d\Phi_{m+1}(p_1, p_2) = \int_0^1 dx' d\Phi_m(x'p_1, p_2) d\Phi_{+1}(x'; p_1, p_2) \quad (2.29)$$

where the radiation phase-space $d\Phi_{+1}$ is

$$d\Phi_{+1}(x'; p_1, p_2) = \frac{2p_1 \cdot p_2}{16\pi^2} dx \delta(x - x') dv \frac{d\phi}{2\pi} \Theta[0 < x < 1] \Theta[0 < v < 1 - x]. \quad (2.30)$$

Further details may be found in [41, 42, 47].

For initial–initial splittings the shower proceeds from the hard process by ‘backwards evolution’ [48], identifying in each splitting a higher-scale parton within the parent hadron. Accordingly, the shower densities depend on both the splitting dipoles and upon the relevant PDFs, evaluated at their respective momentum fractions:

$$P_m^{(ab)}(\Phi_{+1}; \xi_1, \xi_2) = \frac{f_a(\frac{\xi_1}{x}, \mu^{(ab)})}{f_b(\xi_1, \mu^{(ab)})} S^{ab}(x). \quad (2.31)$$

For a $pp \rightarrow X$ process whose only Born partonic subprocess is $q\bar{q} \rightarrow X$, the ‘one-emission’ expansion of the shower applied to the Born matrix-element $B_{q\bar{q}}$ is therefore⁴

$$\begin{aligned} d\hat{\sigma}_{q\bar{q}}^{\text{LO+PS}_1}[\mathcal{O}](\xi) &= d\Phi_m \frac{1}{2\hat{s}_{12}} B_{q\bar{q}}(\Phi_m) \left\{ \Delta_{p_T^{\text{cut}}}^{Q(\Phi_m)} \mathcal{O}(\Phi_m) \right. \\ &+ d\Phi_{+1}^{\text{II}_1} \Theta[p_T^{\text{cut}} < p_{T,1} < Q(\Phi_m)] \Delta_{p_{T,1}}^{Q(\Phi_m)}(\xi) \Delta_{p_T^{\text{cut}}}^{p_{T,1}} \left(\Phi_{m+1}^{\text{II}_1}; \frac{\xi_1}{x}, \xi_2 \right) \left[\frac{\alpha_s(\mu^{\text{II}_1})}{2\pi} \sum_{a \in \{q,g\}} \frac{f_a(\frac{\xi_1}{x}, \mu^{\text{II}_1})}{f_q(\xi_1, \mu^{\text{II}_1})} S^{qa}(x) \mathcal{O}(\Phi_{m+1}^{\text{II}_1}) \right] \\ &+ d\Phi_{+1}^{\text{II}_2} \Theta[p_T^{\text{cut}} < p_{T,1} < Q(\Phi_m)] \Delta_{p_{T,1}}^{Q(\Phi_m)}(\xi) \Delta_{p_T^{\text{cut}}}^{p_{T,1}} \left(\Phi_{m+1}^{\text{II}_2}; \xi_1, \frac{\xi_2}{x} \right) \left[\frac{\alpha_s(\mu^{\text{II}_2})}{2\pi} \sum_{b \in \{q,g\}} \frac{f_b(\frac{\xi_2}{x}, \mu^{\text{II}_2})}{f_{\bar{q}}(\xi_2, \mu^{\text{II}_2})} S^{qb}(x) \mathcal{O}(\Phi_{m+1}^{\text{II}_2}) \right] \left. \right\}, \end{aligned} \quad (2.32)$$

where p_T^{cut} is the shower cut-off scale, $p_{T,1}$ the transverse momentum of the generated emission, and $Q(\Phi_m)$ denotes the shower starting-scale. Note that if the shower algorithm is allowed to proceed, subsequent emissions are only generated at higher orders of α_s , so this is also the perturbative expansion of the full shower to NLO.

For consistency with subsequent sections, we redistribute these terms according to their initial-state partonic channel after the shower emission, and expand in α_s .⁵

$$d\hat{\sigma}_{q\bar{q}}^{\text{LO+PS}_1(0)}[\mathcal{O}](\xi) = d\Phi_m \frac{1}{2\hat{s}_{12}} \left[B_{q\bar{q}}(\Phi_m) \right] \Theta_{\text{cut}}[\Phi_m] \Delta^{(0)}|_{p_T^{\text{cut}}}^{Q(\Phi_m)} \mathcal{O}(\Phi_m) \quad (2.33)$$

$$d\hat{\sigma}_{q\bar{q}}^{\text{LO+PS}_1(1)}[\mathcal{O}](\xi) = d\Phi_m \frac{1}{2\hat{s}_{12}} \left[B_{q\bar{q}}(\Phi_m) \right] \Theta_{\text{cut}}[\Phi_m] \Delta^{(1)}|_{p_T^{\text{cut}}}^{Q(\Phi_m)} \mathcal{O}(\Phi_m) \quad (2.34)$$

$$\begin{aligned} &+ d\Phi_{m+1} \frac{1}{2\hat{s}_{12}} \left[\sum_{i=1}^2 B_{q\bar{q}}(\tilde{\Phi}_m^{\text{II}_i}) \Theta_{\text{cut}}[\tilde{\Phi}_m^{\text{II}_i}] \Theta_{p_T^{\text{cut}}}^{Q(\tilde{\Phi}_m^{\text{II}_i})}(\tilde{\Phi}_m^{\text{II}_i}) S^{qig}(x) \Delta^{(0)}|_{p_{T,1}}^{Q(\tilde{\Phi}_m^{\text{II}_i})}(\tilde{\Phi}_m^{\text{II}_i}; \xi^{\text{II}_i}) \right] \Delta^{(0)}|_{p_T^{\text{cut}}}^{p_{T,1}} \mathcal{O}(\Phi_{m+1}) \\ d\hat{\sigma}_{qg}^{\text{LO+PS}_1(1)}[\mathcal{O}](\xi) &= d\Phi_{m+1} \frac{1}{2\hat{s}_{12}} B_{q\bar{q}}(\tilde{\Phi}_m^{\text{II}_2}) \Theta_{\text{cut}}[\tilde{\Phi}_m^{\text{II}_2}] \\ &\quad \times \Theta_{p_T^{\text{cut}}}^{Q(\tilde{\Phi}_m^{\text{II}_2})} S^{gq}(x) \Delta^{(0)}|_{p_{T,1}}^{Q(\tilde{\Phi}_m^{\text{II}_2})}(\tilde{\Phi}_m^{\text{II}_2}; \xi_1, x\xi_2) \Delta^{(0)}|_{p_T^{\text{cut}}}^{p_{T,1}} \mathcal{O}(\Phi_{m+1}) \end{aligned} \quad (2.35)$$

⁴Note that these are not strictly ‘purely’-partonic differential cross-sections, despite the $d\hat{\sigma}$ notation, as the initial-state backward-evolution of the parton-shower induces an explicit dependence on the partonic momentum fractions through the ratios of PDFs within the splitting densities.

⁵The $\mathcal{O}(\alpha_s^0)$ contribution to the Sudakov factor, $\Delta^{(0)}|_{t_0}^{t_1}(\Phi; \xi)$, is retained to allow the convenient deduction of contributions arising at higher orders, but as implied by eq. (2.18) is exactly 1.

Here and in subsequent similar expressions, we omit factors of the form

$$\frac{f_q(\xi_1, \mu_F(\tilde{\Phi}_m^{\text{II}_1}))}{f_q(\xi_1, \mu^{\text{II}_1})} \frac{f_q(\frac{\xi_1}{x}, \mu^{\text{II}_1})}{f_q(\frac{\xi_1}{x}, \mu_F(\Phi_{m+1}))} \frac{f_{\bar{q}}(\xi_2, \mu_F(\tilde{\Phi}_m^{\text{II}_1}))}{f_{\bar{q}}(\xi_2, \mu_F(\Phi_{m+1}))} = 1 + O(\alpha_s) \quad (2.36)$$

or similar, arising from the initial generation of the Born process and the PDF ratio within the shower emission eq. (2.31) and

$$\frac{\alpha_s(\mu_1)}{\alpha_s(\mu_2)} = 1 + O(\alpha_s) \quad (2.37)$$

arising from the difference in strong-coupling scale between the expansion convention of eq. (2.2) and that chosen for the shower kernels eq. (2.20).

NLO matching⁶

The objective of NLO matching is to retain perturbative accuracy but combine it with the logarithmic resummation of a parton shower. This problem has previously been solved in general by the MC@NLO [1] and POWHEG [2–4] methods.

Concretely, we require that for an infrared-safe observable \mathcal{O} and a suitable choice of generation cuts, matched predictions for its expectation value differ from their NLO fixed-order counterpart by terms that are higher-order in α_s , or by terms which give power-corrections (i.e. non-logarithmic) in the cut-off scale upon integration. That is, for the expectation-value of \mathcal{O} calculated via some matching scheme, we adopt as an ‘NLO matching condition’ that

$$\sigma^{\text{NLO+PS}(0)}[\mathcal{O}](P_1, P_2) = \sigma^{(0)}[\mathcal{O}](P_1, P_2) \quad (2.38)$$

$$\sigma^{\text{NLO+PS}(1)}[\mathcal{O}](P_1, P_2) = \sigma^{(1)}[\mathcal{O}](P_1, P_2) + O\left(\left(\frac{p_T^{\text{cut}}}{\sqrt{s}}\right)^2\right) \quad (2.39)$$

where the expectation value for \mathcal{O} implied by a given differential cross-section is

$$\langle \mathcal{O} \rangle \equiv \sigma[\mathcal{O}](P_1, P_2) \equiv \int d\sigma[\mathcal{O}](P_1, P_2). \quad (2.40)$$

The MC@NLO method (‘subtractive matching’) uses the shower approximation to the real matrix-elements itself as the subtraction term, except below a cutoff where it switches to the exact dipole subtraction to ensure exact cancellation of the infrared divergences of the real-emission matrix-element in its singular limits. In our case, using dipole subtraction and the dipole shower, and for colour-singlet processes, the contribution generated by the shower coincides with the subtraction term.

The subtracted real events generated from the Φ_{m+1} phase-space (‘H-events’) are used as an initial condition for the shower evolution separately from the combined Born, virtual, and integrated subtraction-term events generated from the Φ_m phase-space (‘S-events’), i.e.:

⁶This section is based on ongoing work in collaboration with Simon Plätzer [49] and may be read in companion with the corresponding section of [50].

$$\begin{aligned}
d\hat{\sigma}_{ab}^{\text{MC@NLO}}[\mathcal{O}](\xi) &= d\Phi_m \frac{1}{2\hat{s}_{12}} \left[B_{ab}(\Phi_m) \right] \Theta_{\text{cut}}[\Phi_m] \text{PS}[\mathcal{O}](\Phi_m; \xi) \\
&+ \left(\frac{\alpha_s(\mu_R)}{2\pi} \right) \left\{ d\Phi_m \frac{1}{2\hat{s}_{12}} \left[V_{ab}(\Phi_m) + \sum_{(\alpha)} B_{ab}^{(\alpha)}(\Phi_m) \int d\Phi_{+1}^{(\alpha)} \Theta_{t_0}^{t_1(\Phi_m)} P_m^{(\alpha)}(\Phi_{+1}^{(\alpha)}; \xi^{(\alpha)}) \right. \right. \\
&\quad \left. \left. + \sum_{(\alpha)} B_{ab}^{(\alpha)}(\Phi_m) \int d\Phi_{+1}^{(\alpha)} \Theta_0^{t_0} x S^{(\alpha)}(\Phi_{+1}^{(\alpha)}) \right] \Theta_{\text{cut}}[\Phi_m] \text{PS}[\mathcal{O}](\Phi_m; \xi) \right. \\
&+ d\eta_1 d\eta_2 d\Phi_m (\eta_1 \xi_1 P_1, \eta_2 \xi_2 P_2) \frac{1}{2\hat{s}_{12}} C_{ab}^{\text{FS}}(\eta_1, \eta_2; \mu_F; \Phi_m) \Theta_{\text{cut}}[\Phi_m] \text{PS}[\mathcal{O}](\Phi_m; \eta_1 \xi_1, \eta_2 \xi_2) \\
&+ d\Phi_{m+1} \frac{1}{2\hat{s}_{12}} \left[R_{ab}(\Phi_{m+1}) \Theta_{\text{cut}}[\Phi_{m+1}] \right. \\
&\quad - \sum_{(\alpha)} \Theta_{t_0}^{t_1(\tilde{\Phi}_m^{(\alpha)})} P_m^{(\alpha)}(\Phi_{m+1}; \xi) B^{(\alpha)}(\tilde{\Phi}_m^{(\alpha)}) \Theta_{\text{cut}}[\tilde{\Phi}_m^{(\alpha)}] \\
&\quad \left. - \sum_{(\alpha)} \Theta_0^{t_0} S^{(\alpha)}(\tilde{\Phi}_{+1}^{(\alpha)}) B^{(\alpha)}(\tilde{\Phi}_m^{(\alpha)}) \Theta_{\text{cut}}[\tilde{\Phi}_m^{(\alpha)}] \right] \text{PS}[\mathcal{O}](\Phi_{m+1}; \xi) \left. \right\} \\
&+ \mathcal{O}(\alpha_s^2).
\end{aligned} \tag{2.41}$$

The effects of this in practice have been explored in detail in [10, 11, 14, 15, 27] and applied for phenomenological studies throughout the operation of the LHC.

Reorganised by order in α_s and by their contribution to $\mathcal{O}(\Phi_m)$ and $\mathcal{O}(\Phi_{m+1})$, the contributions arising up to NLO within MC@NLO for colour-singlet processes are:

$$d\hat{\sigma}_{q\bar{q}}^{\text{MC@NLO}(0)}[\mathcal{O}] = d\Phi_m \frac{1}{2\hat{s}_{12}} \left[B_{q\bar{q}}(\Phi_m) \right] \Theta_{\text{cut}}[\Phi_m] \Delta^{(0)}|_{p_T^{\text{cut}}}^{Q(\Phi_m)} \mathcal{O}(\Phi_m) \tag{2.42}$$

$$\begin{aligned}
d\hat{\sigma}_{q\bar{q}}^{\text{MC@NLO}(1)}[\mathcal{O}] &= d\Phi_m \frac{1}{2\hat{s}_{12}} \left[B_{q\bar{q}}(\Phi_m) \Delta^{(1)}|_{p_T^{\text{cut}}}^{Q(\Phi_m)} + \left\{ V_{q\bar{q}}(\Phi_m; \mu_R) + I_{q\bar{q}}(\Phi_m; \mu_R) \right. \right. \\
&\quad \left. \left. - B_{q\bar{q}}(\Phi_m) \sum_{(\alpha)} \int d\Phi_{+1}^{(\alpha)} \Theta_{Q(\Phi_m)}^{\infty} x S^{(\alpha)}(\Phi_{+1}^{(\alpha)}) \right\} \Delta^{(0)}|_{p_T^{\text{cut}}}^{Q(\Phi_m)} \right] \Theta_{\text{cut}}[\Phi_m] \mathcal{O}(\Phi_m) \\
&+ d\eta_1 d\eta_2 d\Phi_m (\eta_1 \xi_1 P_1, \eta_2 \xi_2 P_2) \frac{1}{2\hat{s}_{12}} \left[\left(P(\mu_F) + K^{\text{FS}} \right)_{q\bar{q}} (\eta_1) B_{q\bar{q}}(\Phi_m) \delta_{\eta_2}^1 \right. \\
&\quad \left. + \delta_{\eta_1}^1 B_{q\bar{q}}(\Phi_m) \left(P(\mu_F) + K^{\text{FS}} \right)_{q\bar{q}} (\eta_2) \right] \Theta_{\text{cut}}[\Phi_m] \Delta^{(0)}|_{p_T^{\text{cut}}}^{Q(\Phi_m)} \mathcal{O}(\Phi_m) \\
&+ d\Phi_{m+1} \frac{1}{2\hat{s}_{12}} \left[R_{q\bar{q}}(\Phi_{m+1}) \Theta_{\text{cut}}[\Phi_{m+1}] \Delta^{(0)}|_{p_T^{\text{cut}}}^{Q(\Phi_{m+1})} \right. \\
&\quad + \sum_{i=1}^2 \left(\Theta_{p_T^{\text{cut}}}^{Q(\tilde{\Phi}_m^{\text{II}_i})} \Delta^{(0)}|_{p_{T,1}}^{Q(\tilde{\Phi}_m^{\text{II}_i})} \Delta^{(0)}|_{p_T^{\text{cut}}}^{p_{T,1}}(\Phi_{m+1}) \right. \\
&\quad \left. \left. - \Theta_0^{Q(\tilde{\Phi}_m^{\text{II}_i})} \Delta^{(0)}|_{p_T^{\text{cut}}}^{Q(\Phi_{m+1})} \right) \Theta_{\text{cut}}[\tilde{\Phi}_m^{\text{II}_i}] B_{q\bar{q}}(\tilde{\Phi}_m^{\text{II}_i}) S^{gq}(x) \right] \mathcal{O}(\Phi_{m+1})
\end{aligned} \tag{2.43}$$

$$\begin{aligned}
d\hat{\sigma}_{qg}^{\text{MC@NLO}(1)}[\mathcal{O}] &= d\eta_2 d\Phi_m (\xi_1 P_1, \eta_2 \xi_2 P_2) \frac{1}{2\hat{s}_{12}} B_{q\bar{q}}(\Phi_m) \left(P(\mu_F) + K^{\text{FS}} \right)_{gq} (\eta_2) \\
&\quad \times \Theta_{\text{cut}}[\Phi_m] \Delta^{(0)}|_{p_T^{\text{cut}}}^{Q(\Phi_m)} \mathcal{O}(\Phi_m) \\
&+ d\Phi_{m+1} \frac{1}{2\hat{s}_{12}} \left[R_{qg}(\Phi_{m+1}) \Theta_{\text{cut}}[\Phi_{m+1}] \Delta^{(0)}|_{p_T^{\text{cut}}}^{Q(\Phi_{m+1})} \right. \\
&\quad + \left(\Theta_{p_T^{\text{cut}}}^{Q(\tilde{\Phi}_m^{\text{II}_2})} \Delta^{(0)}|_{p_{T,1}}^{Q(\tilde{\Phi}_m^{\text{II}_2})} \Delta^{(0)}|_{p_T^{\text{cut}}}^{p_{T,1}}(\Phi_{m+1}) \right. \\
&\quad \left. \left. - \Theta_0^{Q(\tilde{\Phi}_m^{\text{II}_2})} \Delta^{(0)}|_{p_T^{\text{cut}}}^{Q(\Phi_{m+1})} \right) \Theta_{\text{cut}}[\tilde{\Phi}_m^{\text{II}_2}] B_{q\bar{q}}(\tilde{\Phi}_m^{\text{II}_2}) S^{gq}(x) \right] \mathcal{O}(\Phi_{m+1})
\end{aligned} \tag{2.44}$$

where we have again omitted ratios of PDFs and of α_s evaluated at different scales.

This can be verified to satisfy the NLO matching condition: the error relative to eq. (2.11) is

$$\Theta_0^{p_T^{\text{cut}}} \times \left[\sum_{(\alpha)} B_{q\bar{q}}(\tilde{\Phi}_m^{(\alpha)}) S^{(\alpha)}(x) \left(\mathcal{O}(\Phi_{m+1}) - \mathcal{O}(\tilde{\Phi}_m^{(\alpha)}) \right) \right], \quad (2.45)$$

which gives a non-logarithmic correction upon integration for IR-safe observable \mathcal{O} . The precise power of the power-correction in eq. (2.39) depends on the rate of convergence of the observable in the unresolved limit. For cross-section-type observables, in which $\mathcal{O}(\Phi) \equiv 1$ (or a product of theta-functions implementing fiducial cuts), this vanishes for sufficiently small cut-off scales, in which case the NLO-matching is exact.

In the interest of pedagogical clarity, we give a brief guided tour of the key features of eqs. (2.42) to (2.44) germane to a comparison with the corresponding dipole-subtracted NLO expressions of eqs. (2.11) and (2.12). The leading-order terms in the expansion of the Sudakov factors, $\Delta^{(0)} \Big|_{p_T^{\text{cut}}}^{Q(\Phi_m)}$, are 1 and, for strict fixed-order comparisons, may be ignored. They are retained purely to facilitate subsequent comparisons between matching schemes, in which the exponential suppression arising from the inclusion of the higher-order terms within eq. (2.18) becomes relevant. The Θ_{cut} factors may also, in practice, be considered to be identically 1 as long as the generator cuts are appropriately chosen for \mathcal{O} (they may only be zero if \mathcal{O} is also zero); they are retained here to allow terms to be identified directly as either ‘H’-events, generated from Φ_{m+1} and therefore accompanied by $\Theta_{\text{cut}}[\Phi_{m+1}]$, or as ‘S’-events generated from Φ_m . This division allows the required cancellations between contributions to be easily identified. Finally, we note that $\Delta^{(1)} \Big|_{p_T^{\text{cut}}}^{Q(\Phi_m)}$ contains contributions corresponding to eq. (2.31) for all possible splittings, and therefore includes terms, proportional to the gluon PDF f_g , which cancel against the (differential) splitting term generated by the parton shower within eq. (2.44).

2.2 The KrkNLO method

The KrkNLO method generates all events from the Born phase-space Φ_m and uses the shower algorithm itself to generate real-type events with Φ_{m+1} kinematics. According to the decision tree implied by the shower algorithm, events are reweighted multiplicatively to introduce the real and virtual matrix-elements, and satisfy the matching condition.

The method may be summarised succinctly as:

```

for all Born events do shower
  if first emission generated, from kernel  $(\alpha)$  then
     $w \leftarrow w \times \frac{R(\Phi_{m+1})}{P_m^{(\alpha)}(\Phi_{m+1})}$ 
  end if
   $w \leftarrow w \times \left[ 1 + \frac{\alpha_s(\mu_R)}{2\pi} \left( \frac{V(\Phi_m; \mu_R)}{B(\Phi_m)} + \frac{I(\Phi_m; \mu_R)}{B(\Phi_m)} + \Delta_0^{\text{FS}} \right) \right]$ 
end for

```

This is possible only because of the Krk factorisation scheme, which will be discussed further in section 2.3; as a consequence of this, no additional collinear convolutions are required at the level of the hard cross-section, and NLO accuracy can be achieved through multiplicative reweighting alone. Within KrkNLO, Δ_0^{FS} is a factorisation-scheme-dependent constant, as will be discussed further in section 2.3.

To $O(\alpha_s)$, the KrkNLO algorithm generates the following contributions:

$$d\sigma_{q\bar{q}}^{\text{KrknLO}(0)}[\mathcal{O}] = d\Phi_m \frac{1}{2\hat{s}_{12}} \left[B_{q\bar{q}}(\Phi_m) \right] \Theta_{\text{cut}}[\Phi_m] \Delta^{(0)} \Big|_{p_T^{\text{cut}}}^{Q(\Phi_m)} \mathcal{O}(\Phi_m) \quad (2.46)$$

$$d\sigma_{q\bar{q}}^{\text{KrknLO}(1)}[\mathcal{O}] = d\Phi_m \frac{1}{2\hat{s}_{12}} \left[B_{q\bar{q}}(\Phi_m) \Delta^{(1)} \Big|_{p_T^{\text{cut}}}^{Q(\Phi_m)} \right. \quad (2.47)$$

$$\begin{aligned} & \left. + \left\{ V_{q\bar{q}}(\Phi_m; \mu_R) + I_{q\bar{q}}(\Phi_m; \mu_R) + \Delta_0^{\text{Krkn}} B_{q\bar{q}}(\Phi_m) \right\} \Delta^{(0)} \Big|_{p_T^{\text{cut}}}^{Q(\Phi_m)} \right] \Theta_{\text{cut}}[\Phi_m] \mathcal{O}(\Phi_m) \\ & + d\eta_1 d\eta_2 d\Phi_m (\eta_1 \xi_1 P_1, \eta_2 \xi_2 P_2) \frac{1}{2\hat{s}_{12}} \left[\left(P(\mu_F) + K^{\overline{\text{MS}} \rightarrow \text{Krkn}} \right)_{qq} (\eta_1) B_{q\bar{q}}(\Phi_m) \delta_{\eta_2}^1 \right. \\ & \quad \left. + \delta_{\eta_1}^1 B_{q\bar{q}}(\Phi_m) \left(P(\mu_F) + K^{\overline{\text{MS}} \rightarrow \text{Krkn}} \right)_{qq} (\eta_2) \right] \Theta_{\text{cut}}[\Phi_m] \Delta^{(0)} \Big|_{p_T^{\text{cut}}}^{Q(\Phi_m)} \mathcal{O}(\Phi_m) \\ & + d\Phi_{m+1} \frac{1}{2\hat{s}_{12}} \left[\frac{R_{q\bar{q}}(\Phi_{m+1})}{B_{q\bar{q}}(\tilde{\Phi}_m^{\text{II}_1}) S^{q_1 g}(x) \Theta_{\text{cut}}[\tilde{\Phi}_m^{\text{II}_1}] + B_{q\bar{q}}(\tilde{\Phi}_m^{\text{II}_2}) S^{q_2 g}(x) \Theta_{\text{cut}}[\tilde{\Phi}_m^{\text{II}_2}]} \right. \\ & \quad \left. \times \left(\sum_{i=1}^2 \Theta_{\text{cut}}[\tilde{\Phi}_m^{\text{II}_i}] \Theta_{p_T^{\text{cut}}}^{Q(\tilde{\Phi}_m^{\text{II}_i})}(\tilde{\Phi}_m^{\text{II}_i}) \Delta^{(0)} \Big|_{p_{T,1}}^{Q(\tilde{\Phi}_m^{\text{II}_i})} \Delta^{(0)} \Big|_{p_T^{\text{cut}}}^{p_{T,1}}(\Phi_{m+1}) B_{q\bar{q}}(\tilde{\Phi}_m^{\text{II}_i}) S^{q_i g}(x) \right) \right] \mathcal{O}(\Phi_{m+1}) \\ d\sigma_{q\bar{q}}^{\text{KrknLO}(1)}[\mathcal{O}] & = d\eta_2 d\Phi_m (\xi_1 P_1, \eta_2 \xi_2 P_2) \frac{1}{2\hat{s}_{12}} B_{q\bar{q}}(\Phi_m) \left(P_{qg}(\mu_F) + K^{\overline{\text{MS}} \rightarrow \text{Krkn}} \right) (\eta_2) \Theta_{\text{cut}}[\Phi_m] \Delta^{(0)} \Big|_{p_T^{\text{cut}}}^{Q(\Phi_m)} \mathcal{O}(\Phi_m) \\ & + d\Phi_{m+1} \frac{1}{2\hat{s}_{12}} R_{qg}(\Phi_{m+1}) \Theta_{\text{cut}}[\tilde{\Phi}_m^{\text{II}_2}] \Theta_{p_T^{\text{cut}}}^{Q(\tilde{\Phi}_m^{\text{II}_2})}(\tilde{\Phi}_m^{\text{II}_2}) \Delta^{(0)} \Big|_{p_{T,1}}^{Q(\tilde{\Phi}_m^{\text{II}_2})} \Delta^{(0)} \Big|_{p_T^{\text{cut}}}^{p_{T,1}}(\Phi_{m+1}) \mathcal{O}(\Phi_{m+1}) \quad (2.48) \end{aligned}$$

Note that here, for consistency with the other sections, we continue with the convention used in eq. (2.1) whereby we write the partonic cross-section in the $\overline{\text{MS}}$ scheme, for convolution with $\overline{\text{MS}}$ PDFs. In practice, as will be discussed further in section 2.3, the KrknNLO method uses its own factorisation scheme, defined by the $K_{ab}^{\overline{\text{MS}} \rightarrow \text{Krkn}}$ terms above, to achieve the NLO matching condition.

For numerical stability we have here chosen the real weight to be

$$\frac{R_{q\bar{q}}(\Phi_{m+1})}{B_{q\bar{q}}(\tilde{\Phi}_m^{\text{II}_1}) S^{q_1 g}(x) \Theta_{\text{cut}}[\tilde{\Phi}_m^{\text{II}_1}] + B_{q\bar{q}}(\tilde{\Phi}_m^{\text{II}_2}) S^{q_2 g}(x) \Theta_{\text{cut}}[\tilde{\Phi}_m^{\text{II}_2}]} \quad (2.49)$$

rather than simply partitioning the real contribution and reweighting each dipole separately,

$$\frac{1}{2} \frac{R_{q\bar{q}}(\Phi_{m+1})}{B_{q\bar{q}}(\tilde{\Phi}_m^{\text{II}_1}) S^{q_1 g}(x)}, \quad \frac{1}{2} \frac{R_{q\bar{q}}(\Phi_{m+1})}{B_{q\bar{q}}(\tilde{\Phi}_m^{\text{II}_2}) S^{q_2 g}(x)} \quad (2.50)$$

for each generated shower emission respectively. In the statistical limit they are equivalent; the inclusion of the second dipole in the denominator regulates the weight distribution when the emitting dipole kernel is small.

From eqs. (2.47) and (2.48) it is clear that for NLO accuracy we require from $\Theta_{p_T^{\text{cut}}}^{Q(\tilde{\Phi}_m)}$ that the shower starting-scale be unrestricted (i.e. a ‘power’ shower [51, 52]); otherwise high- p_T regions of the real-emission phase-space Φ_{m+1} are excluded. This corresponds to $Q(\Phi_m) \equiv \infty$ (in practice we will use $Q_{\text{max}}(\Phi_m)$ to denote the upper-bound arising from kinematic restrictions⁷).

For soft emissions, relative to the fixed-order expression eqs. (2.11) and (2.12), we are also excluding events in which the hardest emission is softer than p_T^{cut} . Assuming this is chosen to be sufficiently small in relation to the relevant hard scales of the process, it acts as a slicing parameter, and below this threshold we are in the singular region in which the dipole factorisation yields a good approximation for the corresponding real matrix element and for any IRC-safe observable $\mathcal{O}(\Phi_{m+1}) = \mathcal{O}(\tilde{\Phi}_m^{(\alpha)})$. The ‘missing’ events with an emission softer than p_T^{cut} are restored by the

⁷The kinematic upper-bound differs between the two II-type dipoles but may be expressed concretely as

$$Q_{\text{max}}(\Phi_m) = \frac{1 - \xi_{\text{min}}}{2\sqrt{\xi_{\text{min}}}} \sqrt{\hat{s}_{12}}$$

where $\xi_{\text{min}} = \min\{\xi_1, \xi_2\}$.

mismatch in integration domains between the integrated dipoles and the implicit integration within the shower Sudakov factor, with an error given by

$$\Theta_0^{p_T^{\text{cut}}} \times \left[\left(\mathbb{R}(\Phi_{m+1}) - \sum_{(\alpha)} \mathbb{B}_{q\bar{q}}^{(\alpha)}(\tilde{\Phi}_m^{(\alpha)}) S^{(\alpha)}(x) \right) \mathcal{O}(\Phi_{m+1}) \right. \\ \left. + \sum_{(\alpha)} \mathbb{B}_{q\bar{q}}^{(\alpha)}(\tilde{\Phi}_m^{(\alpha)}) S^{(\alpha)}(x) \left(\mathcal{O}(\Phi_{m+1}) - \mathcal{O}(\tilde{\Phi}_m^{(\alpha)}) \right) \right]. \quad (2.51)$$

The former term in eq. (2.51) is the difference between the real-emission matrix element \mathbb{R} and its Catani–Seymour dipole-subtraction counterterm, within the singular region regulated by p_T^{cut} . By construction the IR-divergent terms therefore cancel and this term can contribute at most a power-correction (i.e., not logarithmically-enhanced). The latter term is the difference between the measurement function \mathcal{O} for an IRC-safe observable applied to Φ_{m+1} and to a reduced phase-space configuration in which the unresolved particle is mapped away $\tilde{\Phi}_m^{(\alpha)}$, in the unresolved region, and therefore also contributes at most a power-correction [47].

In order to satisfy the NLO matching condition, it is necessary to correctly reproduce the NLO cross-section when setting $\mathcal{O}(\Phi)$ equal to a product of theta-functions implementing fiducial cuts. This requires the factorisation scheme kernels $\mathbb{K}_{ab}^{\overline{\text{MS}} \rightarrow \text{FS}}$ to cancel the collinear contributions generated by the integral of the shower kernels over the radiative phase-space within $\Delta^{(1)} \Big|_{p_T^{\text{cut}}}^{Q(\Phi_m)}$.⁸ This is sufficient for KrkNLO to satisfy the NLO matching condition for general \mathcal{O} . The corresponding factorisation scheme, called the Krk scheme⁹ [30, 32], is introduced in further detail in section 2.3 and appendix B.

Finally, we note that terms contributing to $\mathcal{O}(\Phi_{m+1})$ are generated with identical ‘Born’ Sudakov factors corresponding to the parton-shower probability of generating an emission at that scale, starting from the relevant underlying Born kinematics. Whilst at the order shown these Sudakov factors are 1, the exponential behaviour of eq. (2.18) makes the higher-order contributions of these factors non-negligible, especially where $p_{T,1} \ll Q_{\text{max}}(\tilde{\Phi}_m^{(\alpha)})$. In the high- p_T tail, the KrkNLO and fixed-order predictions should coincide.

2.3 The Krk factorisation scheme

As described in section 2.2, the Krk scheme is defined by the requirement that it cancel the collinear terms arising from the integral over the shower emission kernels within the shower Sudakov factor. Full expressions for the factorisation scheme transformation are given in appendix B.

Given a choice of factorisation scheme with PDFs related to those in the $\overline{\text{MS}}$ scheme by

$$\mathbf{f}^{\text{FS}} = \mathbb{K}^{\overline{\text{MS}} \rightarrow \text{FS}} \otimes \mathbf{f}^{\overline{\text{MS}}}, \quad (2.52)$$

where explicitly

$$f_a^{\text{FS}}(x, \mu_F) = \sum_b \int_x^1 \frac{dz}{z} \mathbb{K}_{ab}^{\overline{\text{MS}} \rightarrow \text{FS}}(z, \mu_F) f_b^{\overline{\text{MS}}}\left(\frac{x}{z}, \mu_F\right) \quad (2.53)$$

and the matrix of convolution kernels $\mathbb{K}_{ab}^{\overline{\text{MS}} \rightarrow \text{FS}}$ has perturbative expansion

$$\mathbb{K}_{ab}^{\overline{\text{MS}} \rightarrow \text{FS}}(z, \mu) = \delta_{ab} \delta(1-z) + \frac{\alpha_s(\mu)}{2\pi} \mathbb{K}_{ab}^{\overline{\text{MS}} \rightarrow \text{FS}}(z) + \mathcal{O}(\alpha_s^2), \quad (2.54)$$

⁸Although we present this for the dipole shower, taking advantage of the explicit phase-space integrations performed for dipole subtraction in [33], it can in principle be extended to other shower algorithms with the integration performed numerically where necessary.

⁹The same factorisation scheme was formerly named the ‘Monte Carlo’ scheme in [28–30].

the NLO partonic cross-section must be transformed correspondingly into the new factorisation scheme to retain NLO accuracy,

$$\begin{aligned} d\hat{\sigma}_{ab}^{\text{FS}(1)}(\xi_1 P_1, \xi_2 P_2) = d\hat{\sigma}_{ab}^{\overline{\text{MS}}(1)} - d\eta_1 d\eta_2 \sum_c \left[K_{ca}^{\overline{\text{MS}} \rightarrow \text{FS}}(\eta_1) d\hat{\sigma}_{cb}^{\overline{\text{MS}}(0)}(\eta_1 \xi_1, \eta_2 \xi_2) \delta_{\eta_2}^1 \right. \\ \left. + \delta_{\eta_1}^1 d\hat{\sigma}_{ac}^{\overline{\text{MS}}(0)}(\eta_1 \xi_1, \eta_2 \xi_2) K_{cb}^{\overline{\text{MS}} \rightarrow \text{FS}}(\eta_2) \right]. \end{aligned} \quad (2.55)$$

For eqs. (2.47) and (2.48) the adoption of the Krk scheme therefore amounts to the cancellation of the $K_{ab}^{\overline{\text{MS}} \rightarrow \text{Krk}}$ convolution terms within the perturbative cross-section, and the convolution of the resulting expressions for $d\hat{\sigma}^{\text{Krk}}$ with Krk-scheme PDFs, for which the scheme-transformation eq. (2.53) has been pre-calculated.

The additional choice of $\mu_F^2 = \hat{s}_{12}$ removes the mass-factorisation terms contained within the P operator, since these terms (eq. (A.4)) are proportional to $\log \mu_F^2 / \hat{s}_{12}$. We make the central choice $\mu_F^2 = \hat{s}_{12}$ throughout. Factorisation scale variation by a constant factor (e.g. following the conventional scale-variation heuristic for estimation of missing-higher-order uncertainties), or by a function of x , is equivalent in this case to a variation of the factorisation scheme and would here arise as a factorisation-scheme uncertainty.¹⁰ Since the impact of factorisation-scale variation is well-understood we do not explore this further here.

By comparison of eqs. (2.47) and (2.48) with eqs. (2.43) and (2.44) it is clear that NLO accuracy is achieved provided that

$$K_{qq}^{\overline{\text{MS}} \rightarrow \text{Krk}}(x) = K_{qq}^{\overline{\text{MS}}}(x) - \frac{1}{2} \Delta_0^{\text{FS}} \delta(1-x). \quad (2.56)$$

$$K_{qg}^{\overline{\text{MS}} \rightarrow \text{Krk}}(x) = K_{qg}^{\overline{\text{MS}}}(x) \quad (2.57)$$

That is, the contribution to $K_{qc}^{\overline{\text{MS}} \rightarrow \text{Krk}}$ with non-trivial x -dependence is fully determined by the integrated Catani–Seymour dipoles, whilst for the flavour-diagonal transition, ‘virtual’ terms proportional to $\delta(1-x)$, i.e. associated solely with the unconvoluted Born phase-space $\Phi_m(\xi_1 P_1, \xi_2 P_2)$, are unconstrained by the requirement that the collinear contributions from K^{FS} are absorbed into the factorisation-scheme transformation. Alternative choices of Δ_0^{FS} therefore define a one-parameter family of factorisation schemes all of which give NLO accuracy. To fix it concretely, for the ‘full’ Krk scheme we follow [30] and impose

$$\sum_a \int_0^1 d\xi \xi f_a^{\text{Krk}}(\xi; \mu_F) = 1 \quad (2.58)$$

as a momentum sum rule [53] on the transformed Krk-scheme PDFs (an earlier ‘DY’ scheme used a flavour sum rule [28]); this is achieved by modifying the flavour-diagonal ‘virtual’ corrections, i.e. fixing Δ_0^{FS} , to impose for each flavour a

$$\sum_b \int_0^1 dz z K_{ab}^{\overline{\text{MS}} \rightarrow \text{Krk}}(z) = 0. \quad (2.59)$$

¹⁰Like the choice of renormalisation or factorisation scale, the choice of factorisation scheme is unphysical. An all-order calculation should therefore be independent of the scheme used. However, at any fixed order of perturbation theory, higher-order terms beyond the claimed level of perturbative accuracy are scheme-dependent. The envelope of predictions arising from alternative choices of factorisation scheme may therefore be considered a theory uncertainty, ‘factorisation-scheme uncertainty’, akin to factorisation- and renormalisation-scale uncertainty. There is no clear metric by which one scheme may be considered intrinsically superior to any other save perhaps perturbative convergence, which may be altered by the addition or removal of (perhaps-large) logarithmic terms from the perturbative cross-section. We defer a detailed discussion of factorisation-scheme uncertainty, both for the Krk scheme and for other proposed alternatives to the ‘default’ $\overline{\text{MS}}$ -scheme, to future work.

The ‘full’ Krk scheme further includes an additional redefinition of the gluon PDF derived from gg -channel processes (see appendix B for details); since this entails a modification of the gluon PDF from the $\overline{\text{MS}}$ PDF at order α_s only, this contributes only $O(\alpha_s^2)$ terms to the class of processes considered here and is therefore irrelevant to the NLO matching condition.

As a result of the factorisation scheme and factorisation scale choices, there are no remaining collinear terms, allowing NLO accuracy to be achieved within the hard process solely by multiplicative reweighting with no additional collinear convolutions.

Explicit expressions for the PDF convolution transformation into the Krk scheme are given in appendix B together with a description of the way the transformation is performed in practice; the numerical effect of the transformation of $\overline{\text{MS}}$ PDFs into the Krk factorisation scheme is shown in fig. 8.

2.4 Comparison with MC@NLO

Comparison of the $O(\alpha_s)$ contributions to the matched KrkNLO differential cross-section (eqs. (2.47) and (2.48)) with their MC@NLO counterparts (eqs. (2.43) and (2.44)) is instructive and illustrates the underlying cause of some of the numerical differences between the matching schemes which will emerge at a formally higher-order in α_s despite both satisfying the NLO matching condition and using identical shower algorithms, physics parameters, and underlying $\overline{\text{MS}}$ PDF sets. We briefly highlight these here.

The KrkNLO method requires the phase-space for the first parton shower emission to be unrestricted (a ‘power’ shower), i.e. uses a starting-scale $Q_{\text{max}}(\Phi_m)$ restricted only by the possible kinematics of the splitting. In MC@NLO the shower starting-scale is typically chosen as a characteristic scale related to the underlying hard process; as usual with such choices, this may be varied as a heuristic to estimate shower uncertainties [15, 54–58]. This difference in $Q(\Phi_m)$ choice between KrkNLO and MC@NLO generates different Sudakov factors associated with emissions from the Born phase-space. This difference will be largest when $Q(\Phi_m) \ll Q_{\text{max}}(\Phi_m)$, with additional suppression for KrkNLO arising from the integral over the shower phase-space excluded within MC@NLO.

The MC@NLO method further requires the additional choice $Q(\Phi_{m+1})$ for the starting-scale for ‘H’-events, in which the shower starts from Φ_{m+1} . This is the scale that defines the Sudakov factor for ‘H’-events and bounds the phase-space for the second and subsequent emissions (in our case, $p_{\text{T},2}, p_{\text{T},3}$ etc.). Where $Q(\Phi_{m+1})$ differs significantly from p_{T}^j ,¹¹ the phase-space available for the second parton-shower emission (and consequently, the associated Sudakov factor) will differ substantially between the two methods.

For MC@NLO, where $p_{\text{T},1} > Q(\Phi_m^{\text{II}_i})$, i.e. the real-emission phase-space inaccessible by the parton shower from the underlying Born, the ‘pure’ real-emission matrix-element is unmodified by shower-subtraction terms or the real-emission generated from ‘S’-events. Notably, for the ‘power’-shower choice of $Q(\Phi_m)$ within MC@NLO, this never occurs. For the phase-space accessible by the shower from the underlying Born, at this order the contributions from the ‘H’ and ‘S’ events cancel, but at higher-orders would be governed by the hierarchy of scales between $Q(\Phi_m)$ and $p_{\text{T},1}$ (for the Born Sudakov applied to the ‘S’-events, absent from the ‘H’-events) and between $Q(\Phi_{m+1})$ and $p_{\text{T},1}$ (for the ‘real-emission’ Sudakov).

Within KrkNLO the $\mathcal{O}(\Phi_{m+1})$ contribution receives a single unified Sudakov factor associated with emissions from the underlying Born process. In MC@NLO contributions are associated with

¹¹Note that for the processes we consider here, the p_{T} relative to the beam axis is the same as the ‘shower p_{T} ’ relative to the emitter–spectator axis in the dipole rest frame, and so $Q(\Phi_{m+1}) = p_{\text{T}}^j$ gives a shower phase-space for the second-emission identical to that arising from the shower p_{T} -ordering in the KrkNLO case. For a general process with contributions from IF/FI/FF dipoles, the p_{T} relative to the beam axis will differ from that relative to a parent dipole.

different Sudakov factors according to the underlying division between ‘H’- and ‘S’-events, which is arbitrary and unphysical [1, 42]. One consequence of this is a reduced Sudakov suppression for MC@NLO where $p_{T,1} \ll Q(\Phi_m^{I_i})$ and, for example, especially where $p_{T,1} \sim p_T^{\text{cut}}$.

The KrkNLO method adopts $\mu_F(\Phi_m)^2 = \hat{s}_{12}$, as described in section 2.3, while the functional form for the factorisation scale in MC@NLO may be chosen freely, and is typically chosen as a characteristic scale related to the underlying hard process. This may be expected to contribute to formally-higher-order deviations in regions of phase-space where the ratio μ_F^2/\hat{s}_{12} is large. This is likely to be especially significant where μ_F is chosen as a p_T -based scale, and for instance in the extremes of rapidity distributions [59].

This factorisation scale is used only for the Born process; since the real-emission is generated by the parton shower, the scales used by the PDFs accompanying the real-emission matrix-element R are $\mu_F(\Phi_m)$ for the spectator PDF, and μ^{I_i} for the emitter PDF. Relative to the MC@NLO method there are therefore factors of the form of eqs. (2.36) and (2.37). In addition, due to the adoption of the Krk scheme for the PDFs used within the parton shower kernels of eq. (2.31) (necessary for the first emission to satisfy the matching condition) further modifies the results relative to the ratio of $\overline{\text{MS}}$ PDFs that arise within the MC@NLO method.

The KrkNLO method generates factors of α_s at NLO and beyond within the shower, which use the renormalisation scale $\mu_R = \mu^{(\alpha)}(\Phi_{+1}^{(\alpha)})$ (by default, within the Herwig dipole shower $\mu^{(\alpha)}(\Phi_{+1}^{(\alpha)})$ is the transverse momentum of the splitting with respect to its parent dipole, though this is modified according to the CMW scheme if enabled [60–62]). Since the real-emission matrix-element is generated as a reweighted shower-emission, this is accompanied by a factor of $\alpha_s(\mu^{(\alpha)}(\Phi_{m+1}^{(\alpha)}))$ unless explicitly reweighted. Within MC@NLO, the factors of α_s associated with R are typically all assigned a renormalisation scale $\mu_R(\Phi_{m+1})$.

The adoption of the Krk factorisation scheme for the KrkNLO calculation is motivated by the NLO matching condition as outlined in section 2.3. Beyond NLO, however, the transformed PDFs defined to satisfy the NLO matching condition are also applied to the real and virtual contributions where they generate additional contributions of $O(\alpha_s^2)$.

The MC@NLO populates the real-emission phase-space directly and may therefore be combined with standard Monte Carlo variance-reduction techniques to efficiently sample the real-emission phase-space. The KrkNLO method uses the shower algorithm to sample from the real-emission phase-space, and so relatively under-samples the high- p_T tail where the emission kernels, derived to be good approximations only in the factorisable singular limit, underestimate the true real matrix-element.

The latter could be resolved, along with the relaxation of the requirement for full phase-space coverage by the parton shower, by a hybrid method KrkMC@NLO (see also [63]) in which the two methods are patched together along a hypersurface within phase-space. This amounts to the insertion of a Θ -function, and its complementary $\bar{\Theta}$ -function, into the two methods, and summing the result. In particular, if this were chosen to remove from the MC@NLO contribution the region of phase-space in which the MC@NLO expressions eqs. (2.43) and (2.44) amount to an over-subtraction, it would fix the problem of negative weights arising within MC@NLO by assigning regions generating negativity to KrkNLO (in which all weights are positive). The matching uncertainty resulting from the above differences could then be assessed as a function of the choice of hypersurface, e.g. by defining a one-parameter family smoothly interpolating between the two methods. We defer this to future studies.

3 Implementation

The algorithm described above has been implemented within Herwig 7 [44, 45, 61, 62], using the Herwig dipole shower. In section 3.1 we outline the general features of the implementation used

for the results presented in sections 4 and 5. We postpone a detailed discussion for an anticipated future public release of the KrkNLO code, for general colour-singlet processes, within Herwig 7.4. In section 3.2 we summarise the validation of the implementation of the diphoton production process, which is the specific process chosen for the present work and the subject of the matching studies in sections 4 and 5. The implementation of the Drell-Yan process described in [28] was derived by factorising production from decay and therefore unsuitable to generalise to arbitrary processes. We performed an independent derivation for $pp \rightarrow \gamma\gamma$ as a stepping-stone on the road to the forthcoming fully general implementation.

The diphoton process is the simplest colour-singlet process with no intrinsic mass-scale or resonance, so can usefully elucidate the differing behaviours of the alternative parton-shower matching methods without being obfuscated by convolution with a resonant matrix-element.

3.1 KrkNLO in Herwig 7

Within the Herwig dipole shower, the KrkNLO algorithm is implemented in practice via the abstract `DipoleEventReweight` class [61], by providing a concrete implementation of its two methods, `weight` and `weightCascade`:

weight applies a multiplicative weight each time an emission is generated. In our case, this weight is non-trivial only for the first emission, in which case it reweights the parton-shower dipole emission kernel according to eq. (2.49) or eq. (2.50).

weightCascade applies a multiplicative weight to the entire shower cascade derived from the Born kinematics Φ_m . This is applied to every event, when the shower algorithm reaches the cutoff scale t_0 , and is therefore applied exactly once (unless the shower is forced to terminate after `NEmissions`). In our case, this calculates and applies the virtual weight implied by eq. (2.47),

$$1 + \frac{\alpha_s(\mu_R(\Phi_m))}{2\pi} \frac{1}{B_{q\bar{q}}(\Phi_m)} \left\{ V_{q\bar{q}}(\Phi_m; \mu_R) + I_{q\bar{q}}(\Phi_m; \mu_R) + \Delta_0^{\text{FS}} B_{q\bar{q}}(\Phi_m) \right\}, \quad (3.1)$$

for the $q\bar{q}$ -channel only.

For testing and validation purposes, the contributions of B, R, V, I and Δ_0^{FS} can each be enabled or disabled independently.

Both `weight` and `weightCascade` allow the renormalisation scales used for the $O(\alpha_s)$ contributions to be set flexibly and independently, or (in the real emission case) to be left at the scale generated by the shower.

The value of Δ_0^{FS} is set according to the `KrkNLOEventReweight:PDF` parameter, which should reflect the factorisation scheme of the PDF set chosen for the hard process. This allows the calculation to be performed in the Krk scheme (both ‘full’ [29, 30] and ‘DY’ [28]) and for validation purposes also allows the calculation to be performed in the $\overline{\text{MS}}$ scheme (i.e. $\Delta_0^{\text{FS}} = 0$), in which case external implementations of the contributions provided by the P and K convolution terms in eqs. (2.47) and (2.48) are required for NLO accuracy.

3.2 Validation

To validate the implementation of the KrkNLO method within Herwig 7 for the diphoton process, we have tested each component independently to verify that it behaves as anticipated and, in the relevant limits, correctly reproduces the required fixed-order components for NLO accuracy.

3.2.1 Real matrix elements

Within the KrkNLO implementation, the hard-coded real-emission matrix elements have been tested phase-space-point by phase-space-point against those provided by `OpenLoops` [64] and `MadGraph` [65], with machine-precision accuracy.

For KrkNLO to achieve NLO accuracy, the weights eqs. (2.49) and (2.50) must further correspond exactly to the momentum mappings and splitting kernels used within the parton shower algorithm, and the underlying Born matrix element used for the LO event generation, in order to correctly reproduce the real matrix element.

To verify this numerically within the KrkNLO code, the shower is truncated to provide exactly one emission and events in which no emissions are generated are vetoed. The relevant Sudakov factor $\Delta|_{p_{T,1}}^{Q(\Phi_m)}(\Phi_m)$ is calculated for each splitting by numerical integration (with Vegas [66]) of the splitting kernels considered within the shower algorithm over the splitting phase-space between the scale of the splitting and the starting-scale used within the shower algorithm, using identical kernels, kinematic limits, and scales (both for the PDF ratios and α_s) as are used in the parton shower algorithm. Each event is then reweighted by $1/\Delta|_{p_{T,1}}^{Q(\Phi_m)}(\Phi_m)$.

By comparison of eqs. (2.47) and (2.48) with eqs. (2.11) and (2.12) it is clear that this should lead to agreement, for any observable, between the differential cross-sections calculated by this procedure and those arising from the real-emission contribution of a fixed-order NLO computation (or equivalently, the LO diphoton-plus-jet process).

This has been verified against Matchbox (with matrix elements from MadGraph) for the partonic $q\bar{q}$ - and qg -channels, and for the physical hadronic pp process in which all partonic channels are summed over. A selection of plots indicating excellent agreement is provided in fig. 9, appendix C.

3.2.2 Virtual matrix elements

Within the KrkNLO code, the hard-coded ε -pole and finite remainders of the one-loop matrix elements have been tested phase-space-point by phase-space-point against those provided by OpenLoops, with machine-precision accuracy for arbitrary μ_R . The I term has additionally been checked against the implementation of the Catani–Seymour I-operator automatically generated by Matchbox, and the poles in the dimensional regulator ε have been verified to cancel against those within V rendering the sum IR-finite. The virtual matrix elements may be isolated for validation purposes within the KrkNLO implementation by setting the shower cut-off t_0 sufficiently high as to ensure $t_0 > \max_{\Phi_m} Q(\Phi_m)$, thus prohibiting any parton-shower radiation. The radiative phase-space is then empty and the shower algorithm is effectively bypassed, giving a Sudakov factor identically equal to 1 for all events (i.e. the $O(\alpha_s)$ contribution $\Delta^{(1)}|_{p_T^{\text{cut}}}^{Q(\Phi_m)}(\Phi_m)$, and all higher-order contributions, vanish). By enabling the V and I contributions and disabling the Born and Δ_0^{FS} contributions, as described in section 3.1, the components contributing to $\mathcal{O}(\Phi_m)$ in eq. (2.47) can be tested numerically at the level of differential cross-sections against those calculated using the automated Matchbox implementation within Herwig, using one-loop matrix elements as given by either OpenLoops or MadGraph (or any other supported one-loop provider). A selection of plots indicating excellent agreement is provided in fig. 10, appendix C.

3.2.3 Krk factorisation scheme

PDFs generated by the convolution code used for [28, 30] have been checked against an independent implementation of the same convolution transformations in a separate code. The Born differential cross-section convoluted with Krk-scheme PDFs has been verified to agree numerically with the collinear contribution defined by the Catani–Seymour P and K operators¹² as implemented in Matchbox within Herwig, i.e. verifying

¹²As discussed in section 2.3, the contribution from the mass-factorisation terms given by the Catani–Seymour P operator at $\mu_F = \hat{s}_{12}$ is in fact zero, but the Matchbox code explicitly calculates both operator contributions, as it would for any other scale choice.

$$\sum_f f_{q_f}^{\text{Krk}}(\hat{s}_{12}) \otimes_{\xi_1} d\Phi_m \frac{1}{2\hat{s}_{12}} B_{q_f \bar{q}_f}(\Phi_m) \left(1 + \frac{\alpha_s(\hat{s}_{12})}{2\pi} \Delta_0^{\text{FS}} \right) \mathcal{O}(\Phi_m) \otimes_{\xi_2} f_{\bar{q}_f}^{\text{Krk}}(\hat{s}_{12}) \quad (3.2)$$

$$= \sum_f f_{q_f}^{\overline{\text{MS}}}(\hat{s}_{12}) \otimes_{\xi_1} d\Phi_m(\eta_1 \xi_1 P_1, \eta_2 \xi_2 P_2) \frac{1}{2\hat{s}_{12}} B_{q_f \bar{q}_f}(\Phi_m) \quad (3.3)$$

$$\left(1 + d\eta_1 d\eta_2 \frac{\alpha_s(\hat{s}_{12})}{2\pi} \left[\left(P(\mu_F) + K^{\text{FS}} \right)_{qq}(\eta_1) \delta_{\eta_2}^1 + \delta_{\eta_1}^1 \left(P(\mu_F) + K^{\text{FS}} \right)_{qq}(\eta_2) \right] \right) \mathcal{O}(\Phi_m)$$

$$\otimes_{\xi_2} f_{\bar{q}_f}^{\overline{\text{MS}}}(\hat{s}_{12}) + O(\alpha_s^2)$$

Plots testing the validity of this relationship numerically are shown in fig. 11 of appendix C. This is a non-trivial cross-check of the interplay between the numerical pre-convolution used for the calculation of the Krk-scheme PDFs, and the equivalent numerical convolution operators used in Matchbox. Overall there is good agreement with a difference of 5–10% emerging at high- $M_{\gamma\gamma}$. Within predictions made by the KrkNLO method this may be considered as a component of the overall ‘missing-higher-order’ perturbative uncertainty.

4 Analysis of NLO matching uncertainty

In this section we explore the consequences of using alternative matching methods for precision phenomenology. As outlined in section 2, NLO accuracy is achieved by several different methods which, even using the same NLO hard-process ingredients and the same parton shower algorithm with the same parameters, will nevertheless give predictions which differ. These differences arise formally at a higher-order in the perturbative expansion, but are not guaranteed to be numerically small. Understanding the magnitude of this ‘matching uncertainty’ is a central requirement for the application of matched NLO + parton shower predictions to precision phenomenology. We focus on the similarities and differences between MC@NLO and KrkNLO.

Prior studies comparing alternative matching methods have focused primarily on neutral-current Drell–Yan and related processes involving the production of a massive vector boson or other massive final-states [5, 10, 14–16, 67–69]. The boson mass scale and the associated resonance entering into such processes inevitably dominate their phenomenology, making a clean comparison of matching and shower effects difficult. We choose to focus instead upon the diphoton production process, as the simplest Standard Model colour-singlet process without an intrinsic mass-scale and lacking a vector-boson resonance.

Concretely, throughout this section we present results with fiducial cuts close¹³ to those used by ATLAS for LHC Run II at 13 TeV [70]:

$$p_T^{\gamma_1} > 40 \text{ GeV}, \quad p_T^{\gamma_2} > 30 \text{ GeV}, \quad (4.1a)$$

$$\Delta R_{\gamma\gamma} > 0.4, \quad |y^\gamma| \in [0, 2.5], \quad (4.1b)$$

$$E_T^{\text{iso}}(r) < 0.1 p_T^\gamma \chi(r; R) \quad \text{within cone } r \leq R = 0.4 \quad (4.1c)$$

and generator cuts

$$p_T^\gamma > 5 \text{ GeV}, \quad |y^\gamma| < 25 \quad (4.2)$$

consistently for all predictions.¹⁴

¹³Most notably, the rapidity interval $1.37 \leq |y^\gamma| \leq 1.52$, corresponding to the transition region between the barrel and end-cap calorimeters, is excluded from the ATLAS fiducial cuts (summarised in eq. (5.1)) but is included here.

¹⁴The relatively low choice of generator cut for p_T^γ is required for KrkNLO as it governs access to the real-emission phase-space by ‘migration’ upon the generation of the first parton-shower emission. Simultaneously, however, this choice leads to the large deviation of the ‘power’-shower MC@NLO prediction from the others, due to its large generator-cut dependence (attributable to larger migration in photon- p_T arising from the emission of harder jets). This can be tamed by a choice of p_T^γ -cut closer to the fiducial cut.

In place of the experimental photon isolation we use smooth-cone (‘Frixione’) isolation [71] with the ‘tight’ isolation parameters from the 2013 Les Houches Accords [72], which corresponds to

$$\chi(r; R) = \left(\frac{1 - \cos r}{1 - \cos R} \right) \equiv \left(\frac{\sin \frac{1}{2}r}{\sin \frac{1}{2}R} \right)^2 \quad (4.3)$$

where $E_T^{\text{iso}}(r)$ is the cumulative transverse isolation energy within (rapidity-azimuth) radius r , calculated as the transverse magnitude of the total momentum of all non-photon particles within a cone of radius r .

Results corresponding to the exact experimental fiducial cuts (summarised in eq. (5.1)) are presented in section 5. Where jet distributions are presented we use the anti- k_T algorithm [73] with clustering radius 0.4 and a p_T cut of 1 GeV.

Throughout we use CT18NLO PDFs [74], either in the $\overline{\text{MS}}$ scheme or transformed into the Krk scheme as described in appendix B. Accordingly, we adopt $\alpha_s(M_Z) = 0.118$ as the input to the running of the strong coupling throughout the hard process, shower, and the KrkNLO code. We use the Herwig 7 default dipole-shower cut-off scale $p_T^{\text{cut}} = 1$ GeV. Within Herwig, we disable both hadronisation and the RemnantDecayer so the final-state of the hard-process is the only source of final-state QCD partons and the hard-process is the only input into the parton shower initial-conditions.

We consistently adopt the renormalisation and factorisation scales

$$\mu_R(\Phi_m) = \sqrt{\hat{s}_{12}} \equiv M_{\gamma\gamma} = \mu_F(\Phi_m) \quad (4.4)$$

$$\mu_R(\Phi_{m+1}) = M_{\gamma\gamma} = \mu_F(\Phi_{m+1}). \quad (4.5)$$

Note that as discussed in section 2.2, within the KrkNLO method, the factorisation scale to be used is fixed by the choice of convolution defining the PDF transformation from the $\overline{\text{MS}}$ to the Krk factorisation scheme. This motivates our adoption of this scale consistently for both KrkNLO and MC@NLO. Within the shower we use the scale $\mu^{(\alpha)} = \|\mathbf{k}_T^{(\alpha)}\|$, the transverse-momentum of the generated splitting relative to the emitter-spectator dipole, for both the ratios of PDFs and for the running of α_s .

For MC@NLO we consider several comparators with varying choices of shower starting scale, concretely:

- a ‘power-shower’ with $Q(\Phi_m) = Q_{\text{max}}(\Phi_m)$ and $Q(\Phi_{m+1}) = Q_{\text{max}}(\Phi_{m+1})$;
- a ‘default’ shower with $Q(\Phi_m) = \sqrt{\hat{s}_{12}} \equiv M_{\gamma\gamma}$ and $Q(\Phi_{m+1}) = p_T^{j_1}$, and
- a ‘DGLAP-inspired’ choice in which the shower starting-scale consistently matches the factorisation scale, here $Q(\Phi_m) = M_{\gamma\gamma}$ and $Q(\Phi_{m+1}) = M_{\gamma\gamma}$.

For the KrkNLO method, the shower starting-scale is fixed to Q_{max} as discussed in section 2.2. Note that the ‘power-shower’ choice for MC@NLO is generally not recommended [58], and is included to enable a direct comparison with KrkNLO.

In section 4.1 we consistently truncate the shower in the Φ_{m+1} phase-space (i.e. for diphoton production, Φ_3); in the terminology of MC@NLO, this corresponds to ‘H’-events with no shower emissions and ‘S’ events with up to one shower emission. At this point the matching between the hard-process and the shower is complete and the subsequent evolution of each event is handled entirely by the parton-shower algorithm, which is the same in both cases.¹⁵

In section 4.2 we allow the shower to run to its final cut-off scale, fully populating the emission phase-space. The same predictions, with the unsimplified ATLAS cuts (and combined with the formally-NNLO gluon-gluon box contribution) are compared to experimental data in section 5.

¹⁵This is subject to the caveat that the shower starting-scale for the first ‘post-matching’ emission, $Q(\Phi_{m+1})$ within MC@NLO, may not match the shower starting-scale for the continuation of the shower, $p_{T,1}$ within KrkNLO.

4.1 First-emission only

As discussed in section 2, the first-emission truncation of alternative matching schemes allows their effect to be compared at the level of the initial conditions each method supplies to the parton shower for subsequent evolution (this is often referred to as a ‘parton-level’ comparison, e.g. in [10]). In this section we augment the analytical comparison of section 2.4 between the one-emission-truncated MC@NLO and KrkNLO methods with a numerical comparison.

In the one-emission case, the scale for the emission of the first shower emission from ‘H’-events, $Q(\Phi_{m+1})$, does not enter the calculation, so the second (‘default’) and third (‘DGLAP’) choices outlined above are formally identical. We therefore combine them here.

We turn concretely to the distributions shown in fig. 1. As expected from the reasoning of section 2.4, the predictions converge with the fixed-order calculation in the large- $p_T^{j_1}$ limit where the Sudakov factor is small and the contribution to $\mathcal{O}(\Phi_{m+1})$ is dominated in both cases by the real-emission matrix-element. This is a desired feature of an NLO matching method (and stands in contrast with the behaviour of POWHEG due to its exponentiation of R/B in the hard region [10]). In the low- $p_T^{j_1}$ region, we see the expected additional Sudakov suppression of the real-emission matrix-element within KrkNLO relative to MC@NLO. This leads to a substantial difference in the amount of soft radiation generated in close-to-Born kinematic configurations.

This effect is isolated double-differentially in fig. 2a, broken into six equal slices of $\Delta\phi_{\gamma\gamma}$. Born-like kinematic configurations require $\Delta\phi_{\gamma\gamma} = \pi$, while small values of $\Delta\phi_{\gamma\gamma}$ are only possible if the diphoton system recoils against a hard jet. The predictions can be seen to agree well in the central four $\Delta\phi_{\gamma\gamma}$ bins. The slight deviations at high- $p_T^{j_1}$ can be seen to arise from the low- $\Delta\phi_{\gamma\gamma}$ slices, in which the diphoton system recoils against a jet, gradually becoming kinematically possible; within each slice the relationship between the predictions is fairly stable, but the compositional effect changes the overall ratio in fig. 1. The low- $p_T^{j_1}$ Sudakov suppression shown in fig. 1 arises solely from the close-to-Born configuration in the final $\Delta\phi_{\gamma\gamma}$ slice, which is the dominant contribution and in which the photons are approximately back-to-back. This is the only slice in which soft gluon radiation is kinematically permitted and it is in this slice that the behaviour of the Sudakov factor at low- $p_T^{j_1}$ drives the deviation between KrkNLO and MC@NLO.

A similar pattern can be seen in fig. 2b, in which once again there is generally good agreement between the methods in the central four $\Delta\phi_{\gamma\gamma}$ bins. In this case the dominant difference arising from the Sudakov factor in the low- $p_T^{j_1}$ region for $\Delta\phi_{\gamma\gamma} \approx \pi$ is smeared across the $d\sigma/dM_{\gamma\gamma}$ distribution, leading to an apparent normalisation difference whose origin is nevertheless again the Sudakov factor which accompanies R in the KrkNLO method. The differences between the MC@NLO predictions arising from the change in shower starting-scale $Q(\Phi_m)$ can also be seen in the lowest $\Delta\phi_{\gamma\gamma}$ bin; the effect arises through both the emission-scale theta-function and the Sudakov factor in eqs. (2.43) and (2.44). This discrepancy is sensitive to the choice of generator cuts in eq. (4.2) and may in practice be tamed by the use of more restrictive generator cuts.

This illustrates the general pattern, which is that for inclusive single-differential distributions, the differing behaviour of the predictions for low $p_{T,1}$ will not be directly observed, manifesting instead as a normalisation difference in regions of phase-space which correspond to a close-to-Born configuration if one exists, or a global normalisation difference if not. This can be seen in the remaining distributions of fig. 1, in particular in the $d\sigma/dy_{j_1}$ distribution.

4.2 Full shower

We turn now to the case of direct relevance to phenomenology, in which the parton shower is allowed to run to completion and populate the full phase-space. We again consider the same ‘power-shower’, ‘default’ and ‘DGLAP’ showers as described above in the MC@NLO case, to understand how the

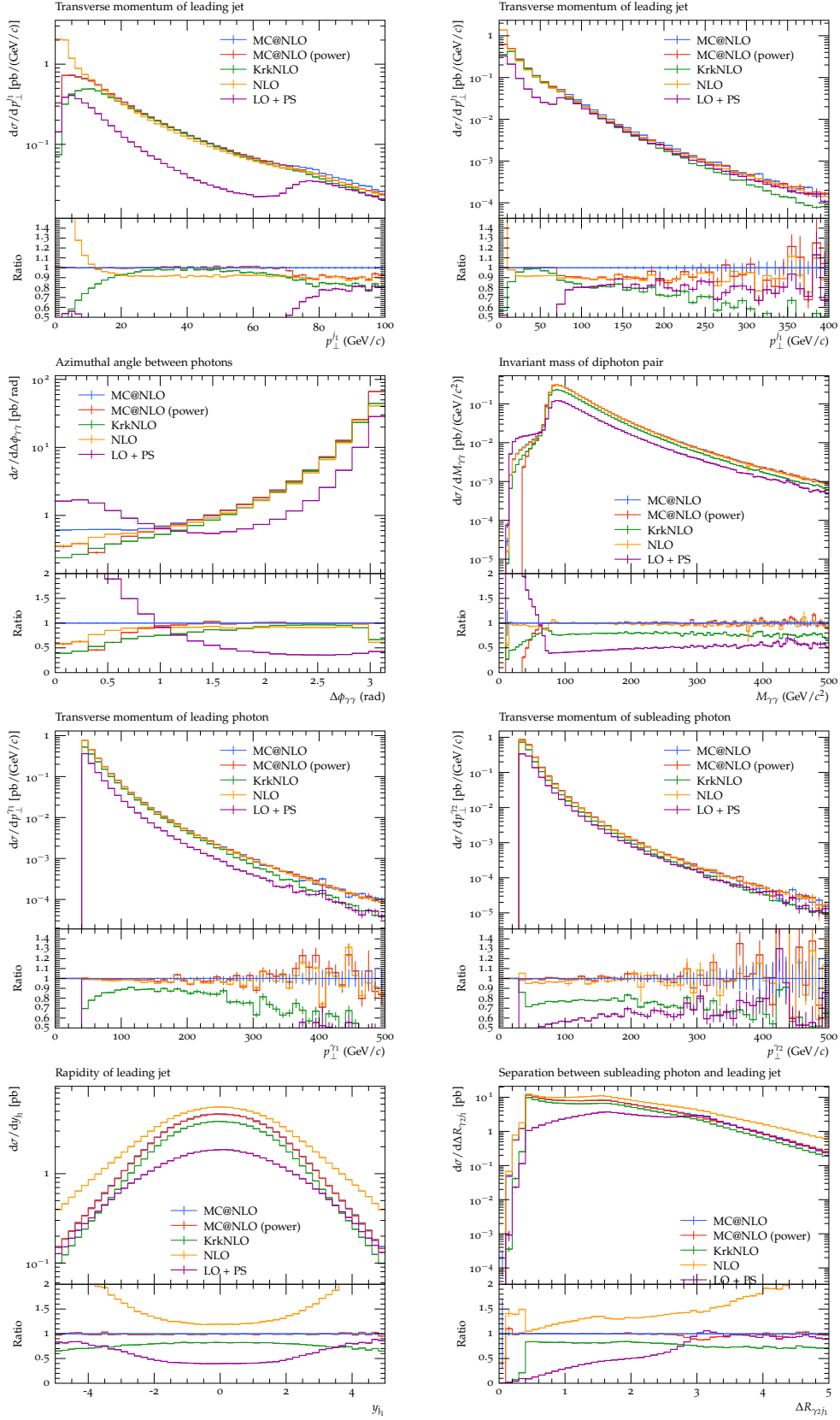
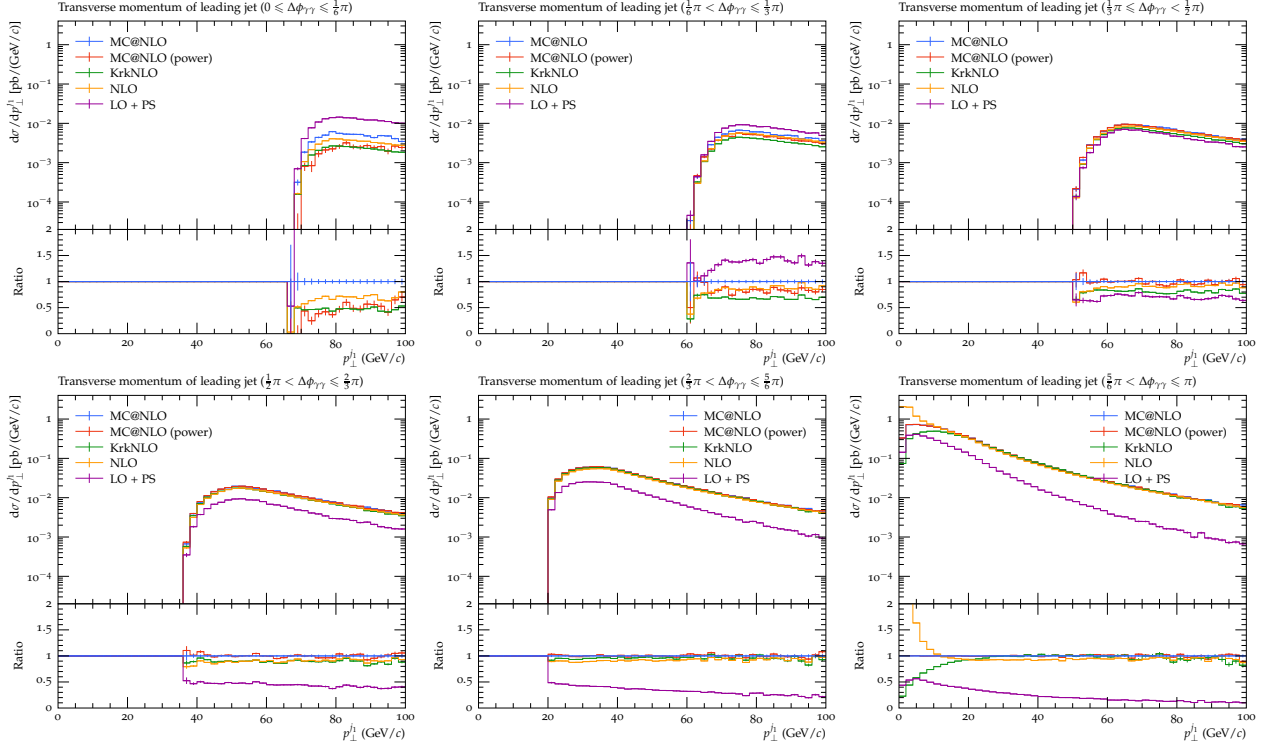
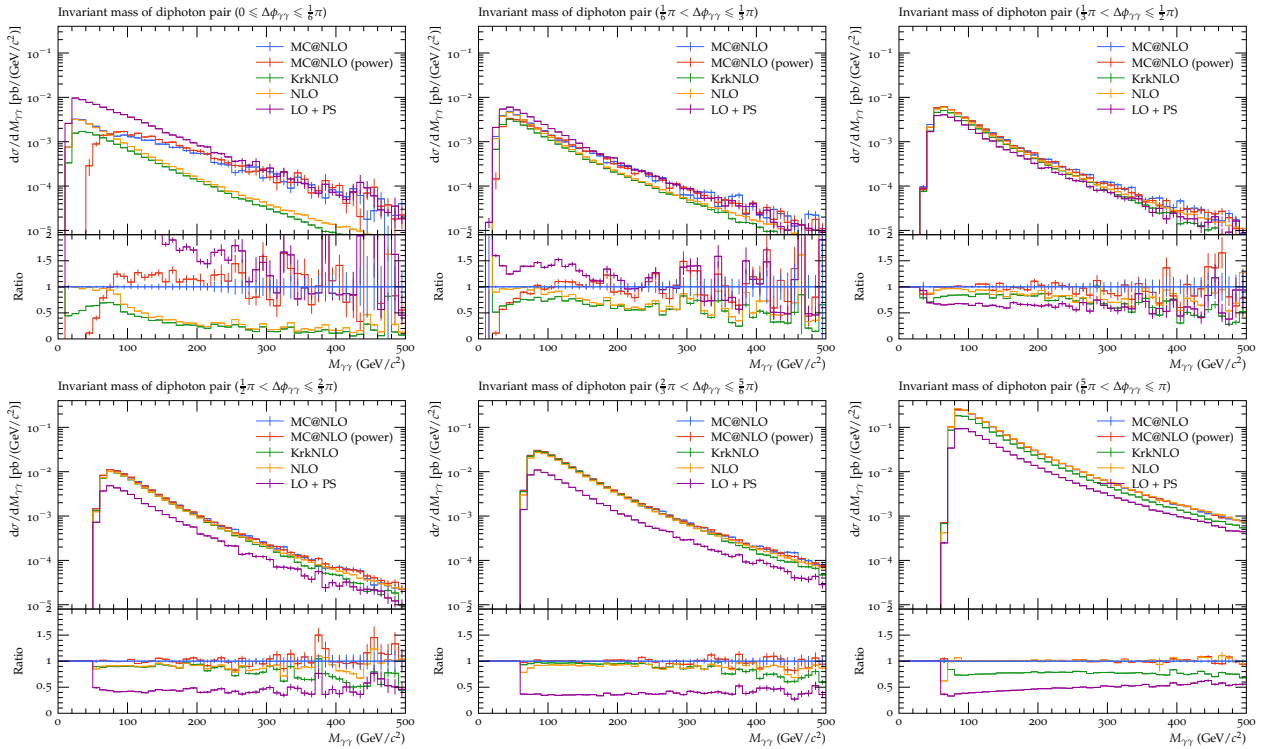


Figure 1: ‘Parton level’ (first-emission) comparison of KrkNLO with MC@NLO, NLO fixed-order, and the corresponding first-emission distributions generated by the parton shower from a leading-order calculation. The shower in each case is a ‘power shower’, i.e. with no phase-space restrictions.



(a) The transverse-momentum distribution of the hardest jet (here, also parton), $d\sigma/dp_T^j$.



(b) The invariant mass distribution of the diphoton pair, $d\sigma/dM_{\gamma\gamma}$.

Figure 2: ‘Parton level’ (first-emission) comparison of differential cross-sections divided into six equal bins of $\Delta\phi_{\gamma\gamma}$, generated by KrkNLO, MC@NLO, NLO fixed-order, and the corresponding first-emission distributions generated by the parton shower from a leading-order calculation.

matching uncertainty between the alternative matching schemes relates to the matching uncertainty arising within MC@NLO due to the choice of the shower starting-scale Q .

In fig. 3 we see that the KrkNLO prediction lies close to the ‘default’ MC@NLO prediction. At high- p_T^j there is a large sensitivity to $Q(\Phi_{m+1})$, but the KrkNLO and ‘default’ MC@NLO choices have qualitatively the same shape and agree moderately well. The ‘power’ shower diverges strongly from the other three choices as has previously been observed in [58], substantially favouring the emission of a hard jet relative to the other matching methods. At lower- p_T^j the KrkNLO method again largely lies between the MC@NLO alternatives.

This region can be studied in further detail in fig. 4a where, as in section 4.1, it is further subdivided according to the value of $\Delta\phi_{\gamma\gamma}$ into six equal slices. As in the one-emission case, at low- p_T^j the overall distribution is dominated by the final slice $\Delta\phi_{\gamma\gamma} \sim \pi$, in which the two photons are approximately back-to-back. In this region we again see the low- $p_{T,1}$ effect of the Sudakov factor applied to R in the KrkNLO method, as in fig. 2. In the MC@NLO method, the Sudakov suppression of R at low- p_T^j is dominated by the Sudakov factor associated with the generation of the second emission, $\Delta|_{p_{T,1}^{\text{cut}}}^{Q(\Phi_{m+1})}$, as shown in eqs. (2.43) and (2.44) and is therefore linked by unitarity to the phase-space available for the generation of the second emission. In this low- $p_{T,1}$ region, for the ‘default’ scale, $Q(\Phi_{m+1}) = p_T^j \sim p_{T,1}^{\text{cut}}$ and so the Sudakov suppression of R is negligible, whilst for the ‘power’ and ‘DGLAP’ choices, $Q(\Phi_{m+1}) \gg p_{T,1}^{\text{cut}}$ generating a Sudakov suppression comparable to that of the KrkNLO method arising instead from the generation of the first shower-emission from the underlying Born. In the ‘default’ case the divergence of the real-emission matrix-element is partially exposed by the miscancellation between the shower-approximation term from the first-emission of the ‘S’-event, which is suppressed by a factor of the Born Sudakov, here

$$\Delta|_{p_{T,1}}^{Q(\tilde{\Phi}_m^{\text{II}_i})}(\tilde{\Phi}_m^{\text{II}_i}) = \Delta|_{p_{T,1}}^{M_{\gamma\gamma}}(\tilde{\Phi}_m^{\text{II}_i}), \quad (4.6)$$

and therefore large, and the dipole-subtraction term from the ‘H’-event, which has no such suppression. Viewed differently, this limit exposes a sensitivity to the finite/non-singular contributions from the dipole terms, which is rendered small when the ‘H’- and ‘S’-event Sudakov factors are similar in magnitude.

In other slices of $\Delta\phi_{\gamma\gamma}$ we see the only identifiable region of phase-space for which the KrkNLO prediction lies outwith the uncertainty envelope implied by the MC@NLO predictions, $\Delta\phi_{\gamma\gamma} \in [0, \frac{1}{6}\pi]$.

Inclusive observables such as $M_{\gamma\gamma}$ are described to NLO accuracy by all the matching set-ups, and might therefore be expected to exhibit reduced matching uncertainty relative to distributions described perturbatively only to leading-order. Invariant-mass-type observables between colour-singlet particles are further privileged by the momentum mappings used within the dipole shower, which leave them unchanged. Each event therefore retains the $M_{\gamma\gamma}$ of the underlying phase-space point of its initial generation (whether Φ_m or Φ_{m+1}) throughout the shower evolution. The differences between the alternatives seen inclusively, as in fig. 3, are unsurprisingly small. In fig. 4b we see the overall distribution is dominated by the final $\Delta\phi_{\gamma\gamma}$ slice in which the distributions agree well. Viewed double-differentially in slices of $\Delta\phi_{\gamma\gamma}$, we can see the effect of the recoil from the additional radiation, which distributes events to slices of $\Delta\phi_{\gamma\gamma}$ according to their subsequent shower evolution. For soft radiation $\Delta\phi_{\gamma\gamma}$ remains unchanged from its Born value, $\Delta\phi_{\gamma\gamma} \approx \pi$, and the alternative schemes agree. Successively harder radiation probes the upper boundary of the shower phase-space, in particular the difference between the ‘DGLAP’ and ‘power’-shower alternatives which emerges only for $\Delta\phi_{\gamma\gamma} \leq \frac{1}{2}\pi$. Intuitively, the additional very-hard-radiation permitted by the power-shower pushes more events into the lowest $\Delta\phi_{\gamma\gamma}$ bins than the alternatives. Once again the KrkNLO prediction lies within the uncertainty envelope of the various MC@NLO predictions, across phase-space, save for the lowest bin of $\Delta\phi_{\gamma\gamma}$.

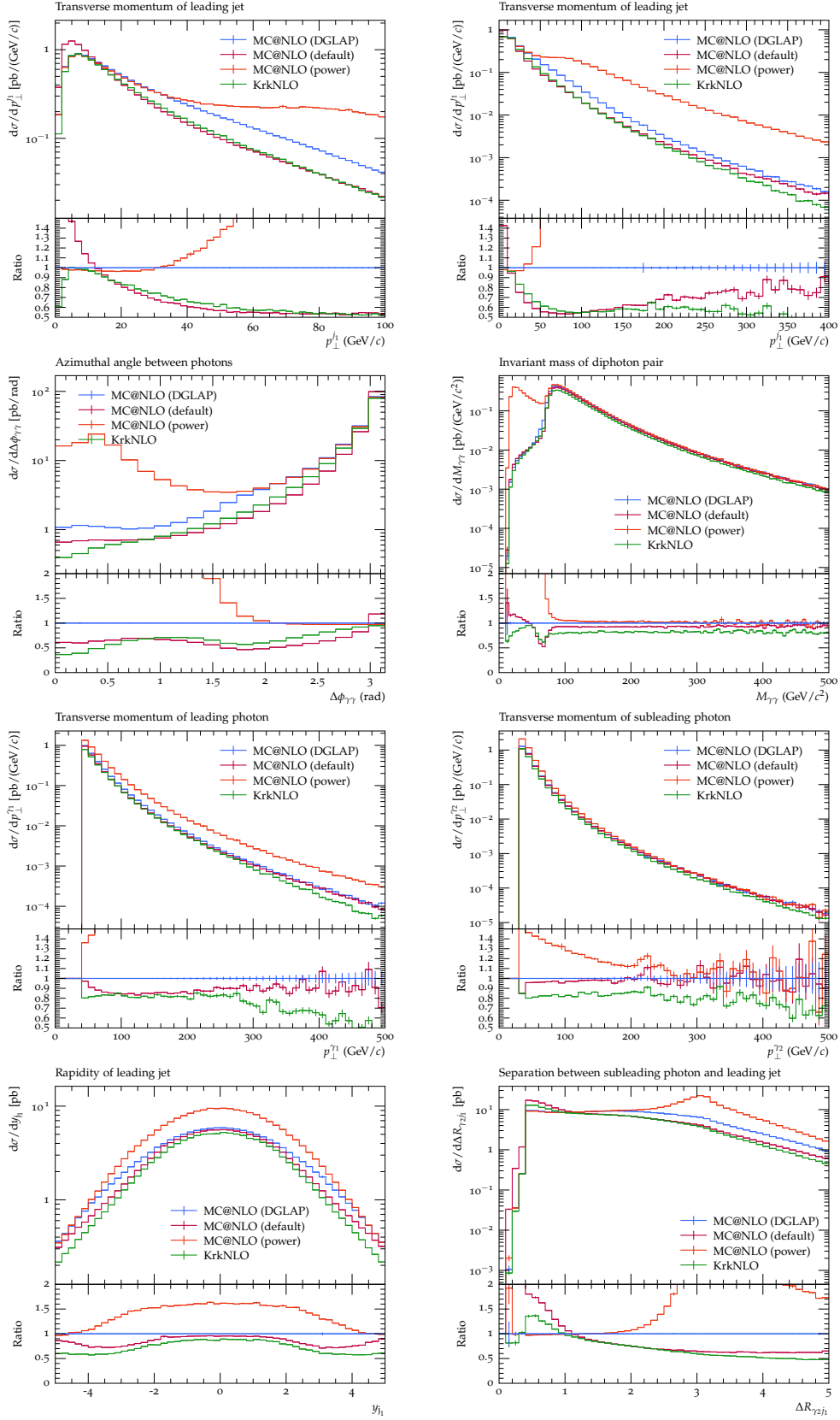
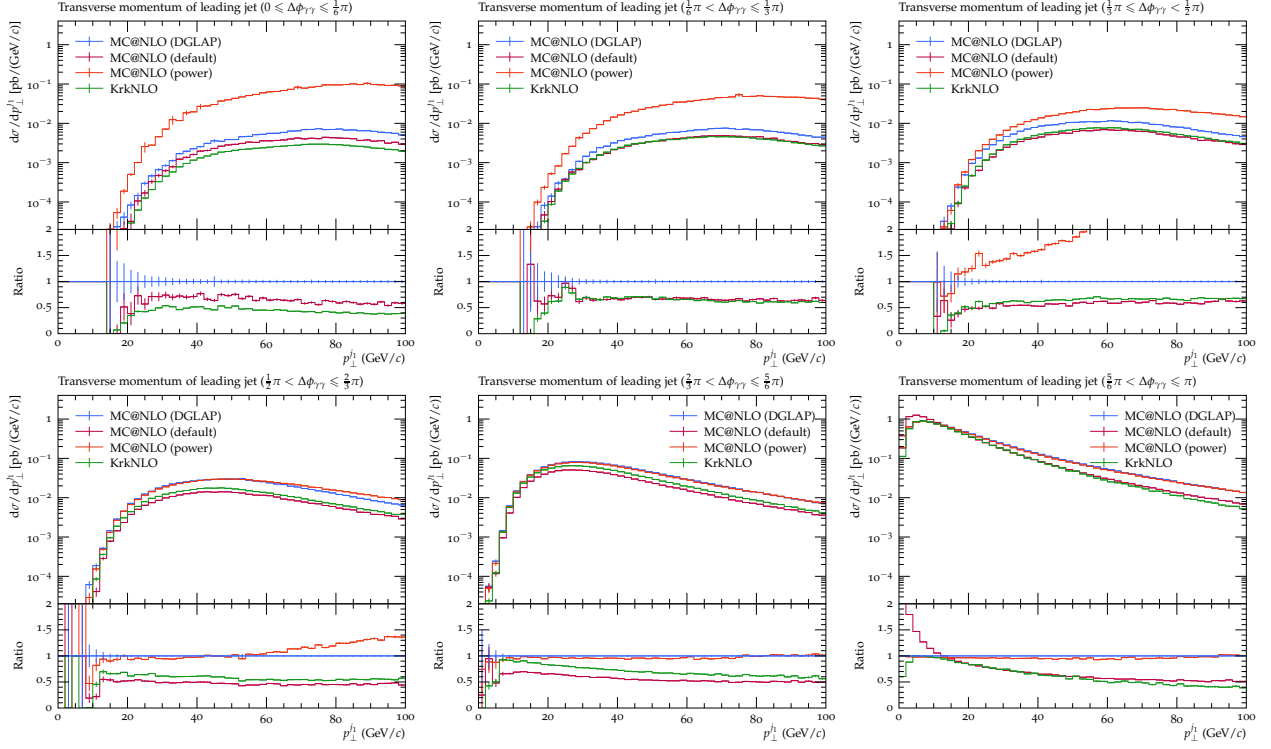
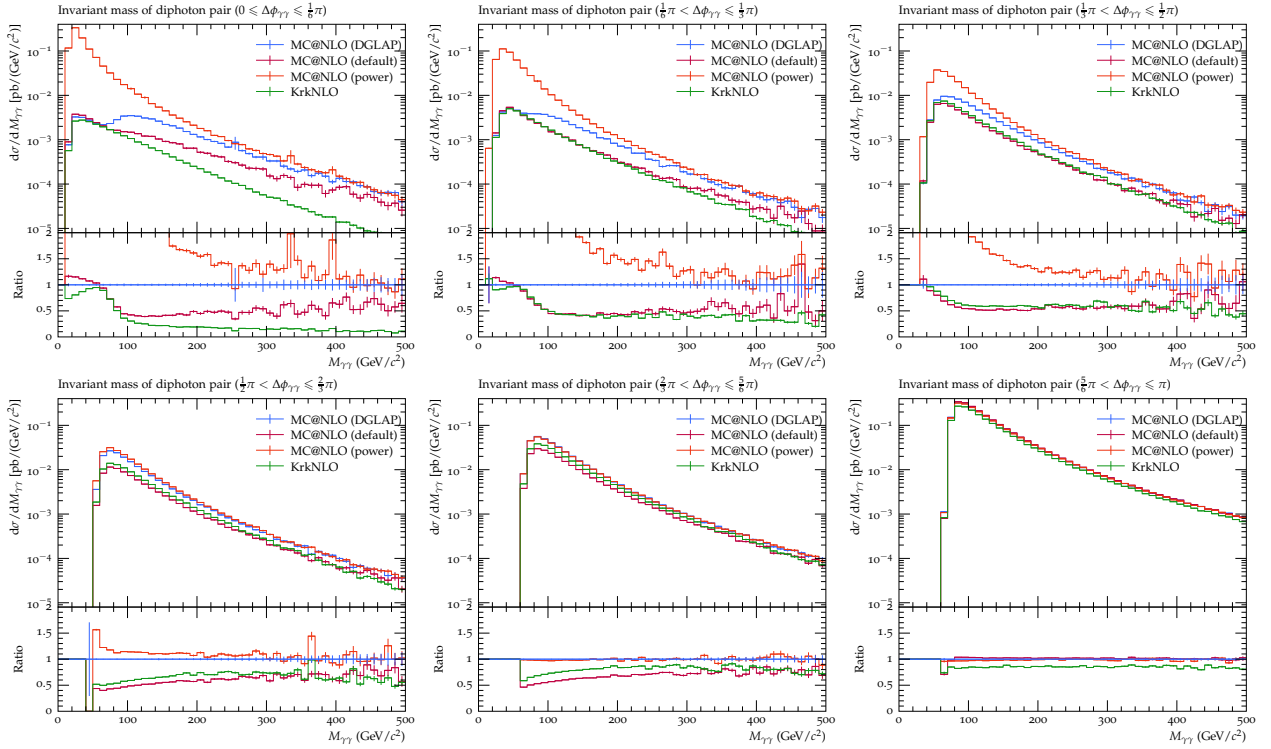


Figure 3: Comparison of matched differential cross-sections generated by KrkNLO and MC@NLO with the ‘default’, ‘power’-shower and ‘DGLAP’ starting-scales.



(a) The transverse-momentum distribution of the hardest jet, $d\sigma/dp_T^j1$.



(b) The invariant mass distribution of the diphoton pair, $d\sigma/dM_{\gamma\gamma}$.

Figure 4: Comparison of matched differential cross-sections divided into six equal bins of $\Delta\phi_{\gamma\gamma}$, generated by KrkNLO and MC@NLO with the ‘default’, ‘power’-shower and ‘DGLAP’ starting-scales.

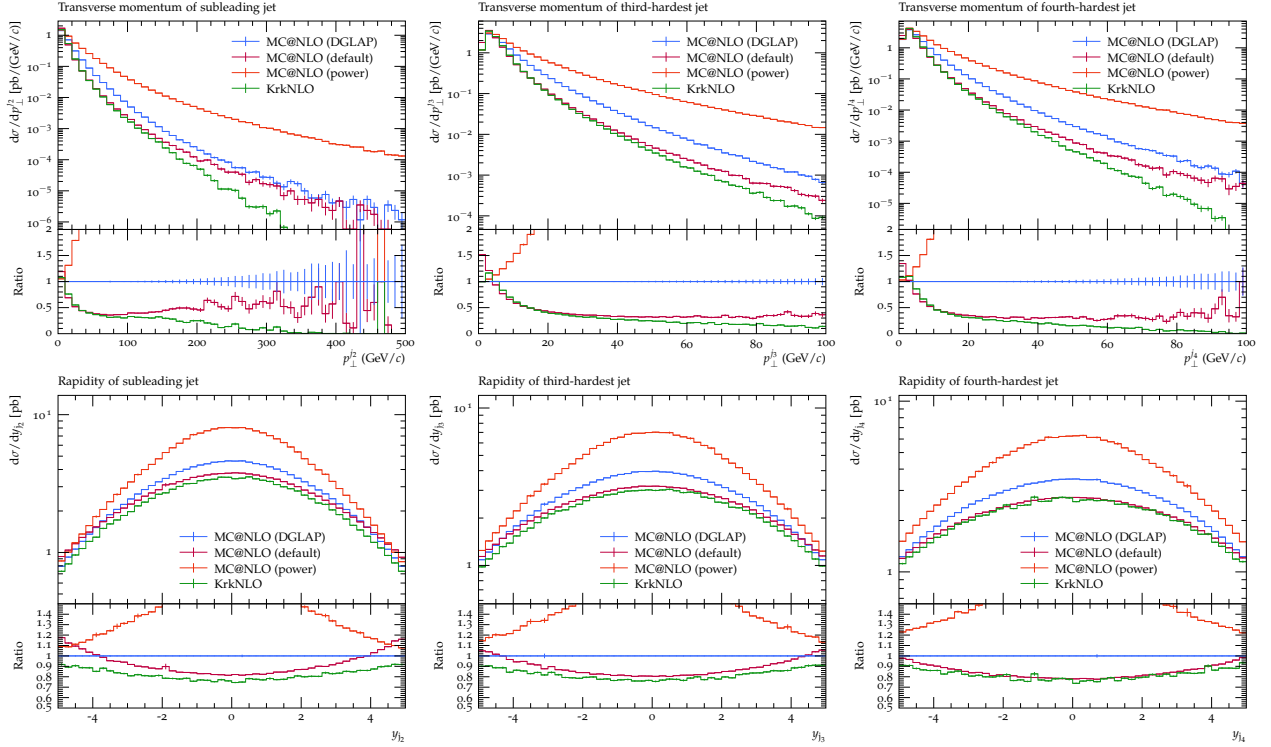


Figure 5: Comparison of matched differential cross-sections with respect to jet transverse momentum and rapidity, generated by KrkNLO and MC@NLO with the ‘default’, ‘power’-shower and ‘DGLAP’ starting-scales.

The distribution with respect to the transverse momenta of the two photons are shown in fig. 3 and are also inclusive distributions, i.e. are calculated to NLO accuracy.¹⁶ Unlike $M_{\gamma\gamma}$, these are sensitive to the transverse momentum of the jet radiation, and like the jet the ‘power’-shower again favours larger values for $p_T^{\gamma 1}$ (against which the jet recoils in a photon-plus-jet type configuration). Again, the KrkNLO prediction lies close to the ‘default’- and ‘DGLAP’ MC@NLO variants. The matching uncertainty for $d\sigma/dp_T^{\gamma 2}$ is considerably smaller, as might be expected.

Finally, distributions of transverse-momentum and rapidity for the additional identified jets are shown in fig. 5. These are not described to any order in perturbation theory and are purely generated by the parton-shower evolution from the initial-conditions provided by the matching method. Again the ‘power’-shower MC@NLO configuration favours harder jets due to the unrestricted $Q(\Phi_{m+1})$, while the KrkNLO and ‘default’ methods agree well, as expected from their similar underlying scale choices.

5 Results and phenomenology

In this section we augment the comparison of section 4 with a comparison of the same predictions against ATLAS 13 TeV data [70], to assess the implications of matching uncertainty for comparisons

¹⁶With the exception of the region $p_T^{\gamma 2} \in [30, 40]$ GeV which is kinematically prohibited at LO by the 2–2 kinematic constraint $p_T^{\gamma 1} = p_T^{\gamma 2}$ and the $p_T^{\gamma 1} > 40$ GeV cut on the hardest photon.

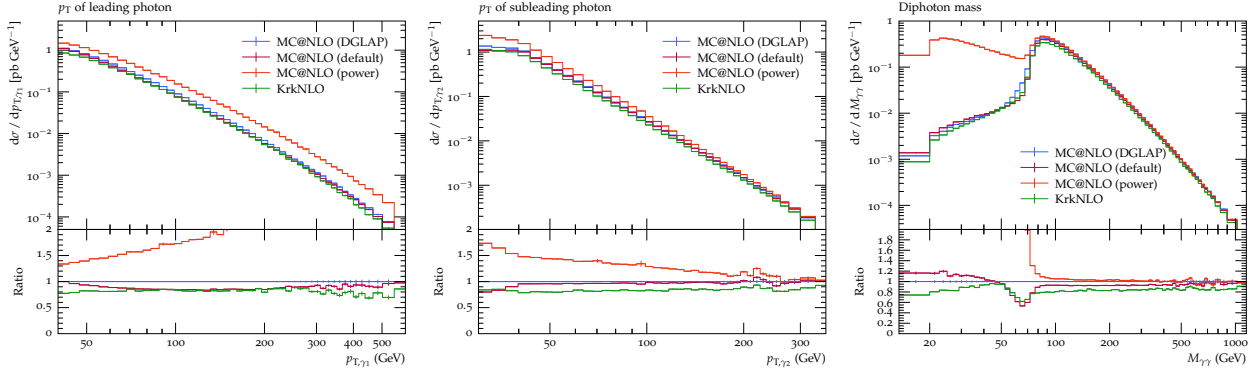


Figure 6: Comparison of matched NLO-plus-parton-shower differential cross-sections as generated by KrkNLO and MC@NLO. Refer to fig. 7 for comparable plots also including ATLAS data.

to data. We use the ATLAS fiducial cuts

$$p_T^{\gamma 1} > 40 \text{ GeV}, \quad p_T^{\gamma 2} > 30 \text{ GeV}, \quad (5.1a)$$

$$\Delta R_{\gamma\gamma} > 0.4, \quad |y^\gamma| \in [0, 1.37] \cup (1.52, 2.37), \quad (5.1b)$$

$$E_T^{\text{iso,part}} < 0.09 p_T^{\gamma} \quad \text{within cone } \Delta R \leq 0.2. \quad (5.1c)$$

implemented in the ATLAS_2021_I1887997 analysis within Rivet [75], where $E_T^{\text{iso,part}}$ is the particle-level transverse isolation energy,¹⁷ and again with generator cuts

$$p_T^{\gamma} > 5 \text{ GeV}, \quad |y^\gamma| < 25 \quad (5.2)$$

consistently for all predictions.

As explained in section 4, the diphoton production process was chosen among the possible Standard Model colour-singlet processes due to its relative kinematic simplicity and absence of intrinsic mass-scales. It is also, however, a process with large NLO and NNLO K -factors, which has been found to require NNLO contributions to provide a good description of data throughout phase-space [59, 76, 77] as well as NNLO contributions to the diphoton-plus-jet process [78], a MINNLO_{PS} calculation [79], or the inclusion of the corresponding multiple-real-emission matrix elements via parton-shower merging methods [80] to give a good description of observables related to the jet-recoil against the diphoton system.

Accordingly, of the ATLAS observables measured in [70] we here present only those which are non-zero at LO and which we can therefore calculate to NLO using KrkNLO. These are nevertheless provided primarily for context and not as an attempt to produce a state-of-the-art prediction.

To improve the numerical comparison with the data, the gluon-gluon box contribution, formally an NNLO contribution relative to the $q\bar{q}$ Born partonic subprocess, has been calculated with Herwig 7 and Matchbox using the one-loop provider GoSam 2.1.1 [81, 82] and is in this section included consistently in all calculations.

These results are shown in fig. 7 (and in fig. 6 without the data). As seen in section 4.2, the matching uncertainty arising within MC@NLO from the shower-scale variation is substantial for the $p_T^{\gamma 1}$ - and $p_T^{\gamma 2}$ -distributions, and much smaller for the $M_{\gamma\gamma}$ distribution.

The latter is poorly-described by the available predictions for most of the available kinematic range, as anticipated by the known requirement for NNLO calculations.

¹⁷ $E_T^{\text{iso,part}}$ is calculated as the excess in the transverse magnitude of the total momentum of all non-photon particles within the isolation cone, over an estimate of the average transverse momentum deposited in a cone of that area due to the underlying event. For more details consult [70] or the corresponding Rivet analysis, ATLAS_2021_I1887997.

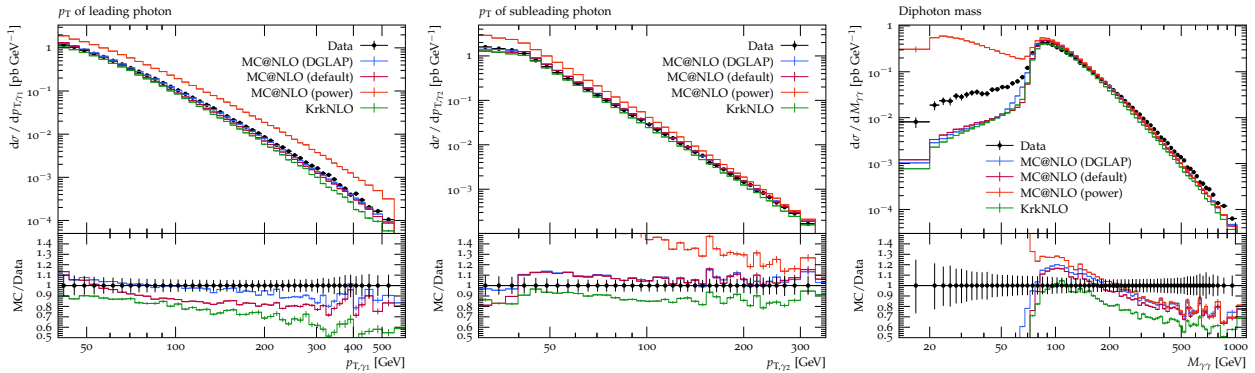


Figure 7: Comparison of matched NLO-plus-parton-shower differential cross-sections as generated by KrkNLO and MC@NLO, to ATLAS data from [70]. The gluon-gluon box contribution (formally NNLO) has been consistently included in all three predictions. The remaining NNLO contributions are significant and their inclusion is required to better describe the data. Refer to fig. 6 for comparable plots without ATLAS data.

The former largely lie within the matching uncertainties of the methods, with good agreement in particular for $d\sigma/dp_T^2$ for the ‘DGLAP’ variant of MC@NLO. However, all the predictions give an acceptable level of agreement considering their limited perturbative accuracy.

6 Conclusion

In this paper we have recapitulated the ‘KrkNLO’ method for the matching of NLO-accurate perturbative calculations of the production of colour-singlet final-states in hadronic collisions to a parton shower, and systematically compared it to one of the main methods in use for LHC phenomenology, the MC@NLO method. Building upon previous work on the KrkNLO method, the formulation presented here is process-independent and can readily be applied to any colour-singlet final-state which proceeds via quark-antiquark annihilation at leading-order.

In comparison to MC@NLO, KrkNLO has the advantage of being fully and unambiguously defined without the need to choose (unphysical) shower starting-scales, the variation of which has been found to lead to large uncertainties [83, 84]. Although heuristics for scale choice have been formulated to reduce this uncertainty [65, 85–88], it remains a potential obstacle to precision phenomenology. The KrkNLO method has no such parameters and therefore no such uncertainty. Despite the very different matching methods used, and the wide range of predictions which may be generated within the MC@NLO method using alternative scale choices, when used with a common choice (and the Herwig default) the MC@NLO and KrkNLO methods are generally found to be in good agreement.

The other method for NLO matching in widespread use, POWHEG, like KrkNLO uses an unrestricted phase-space for the first parton-shower emission, and so avoids MC@NLO’s dependence on an unphysical choice of shower starting-scale. However, in POWHEG this has been found to lead to a transverse-momentum distribution for the first jet that is unreasonably large and is far from that implied by the key NLO ingredient, the real-emission matrix element [6, 11, 86, 89]. In [10] this was attributed to the exponentiation of the R/B contribution throughout the emission phase-space, rather than solely in the singular region in which the universal factorisation behaviour holds. For practical phenomenology, a heuristic has been adopted to fix this in the form of a ‘damping’ function [6] which can be tuned to suppress the exponentiated contribution from the non-singular region and recover the real-emission p_T -distribution. However, this introduces its own intrinsic

uncertainty via the choice of functional form for the damping function and its chosen parameters [13, 69, 90–92]. We emphasise that the KrkNLO method also avoids this uncertainty, despite also using a power-shower. Similarly to MC@NLO, it may be possible to tune the functional form and parameters of the POWHEG damping-function to closely match KrkNLO predictions.

By presenting a formulation of the KrkNLO method suitable for general colour-singlet processes we demonstrate that it is a novel matching method ready for practical LHC phenomenology, with several features making it an interesting and useful complement to MC@NLO and POWHEG. We are currently validating the KrkNLO method for a range of other colour-singlet processes and expect to present further matching comparisons for other processes in future work. We anticipate the public availability of the KrkNLO code within an upcoming release of Herwig 7. Beyond colour-singlets at NLO we remain optimistic about the applicability of a variant of the KrkNLO method to more complex processes and higher-orders.

Acknowledgments

The authors wish to thank Wiesław Płaczek and the late Stanisław Jadach for their work on, and for many fruitful discussions about, the KrkNLO method, and Simon Plätzer for productive discussions about NLO matching, and for his insight into and assistance with Herwig and Matchbox. JW and AS thank Olek Kusina and Stéphane Delorme for valuable discussions about PDF convolutions and factorisation schemes. We are grateful to Wiesław Płaczek, Mike Seymour and Simon Plätzer for their thoughtful comments on the manuscript.

This work was supported by grant 2019/34/E/ST2/00457 of the National Science Centre, Poland. AS is also supported by the Priority Research Area Digiworld under the program ‘Excellence Initiative – Research University’ at the Jagiellonian University in Krakow. We gratefully acknowledge the Polish high-performance computing infrastructure PLGrid (HPC Centre: ACK Cyfronet AGH) for providing computing facilities and support within computational grant PLG/2023/016494.

A Summary of Catani–Seymour insertion operators

For ease of reference, we briefly recap the initial-state insertion operators of Catani–Seymour dipole subtraction that are used for the construction of the KrkNLO matching expressions, largely following the notation of [33].

Parton density functions in the factorisation scheme FS are related to those in the $\overline{\text{MS}}$ scheme by the transformation

$$\mathbf{f}^{\text{FS}} = \mathbb{K}^{\overline{\text{MS}} \rightarrow \text{FS}} \otimes \mathbf{f}^{\overline{\text{MS}}}, \quad (\text{A.1})$$

where explicitly ‘input’ $\overline{\text{MS}}$ PDFs are convolved, locally in μ_{F} , with a kernel,

$$f_a^{\text{FS}}(x, \mu_{\text{F}}) = \sum_b \int_x^1 \frac{dz}{z} \mathbb{K}_{ab}^{\overline{\text{MS}} \rightarrow \text{FS}}(z, \mu_{\text{F}}) f_b^{\overline{\text{MS}}}\left(\frac{x}{z}, \mu_{\text{F}}\right) \quad (\text{A.2})$$

and the matrix of convolution kernels $\mathbb{K}_{ab}^{\overline{\text{MS}} \rightarrow \text{FS}}$ has perturbative expansion

$$\mathbb{K}_{ab}^{\overline{\text{MS}} \rightarrow \text{FS}}(z, \mu) = \delta_{ab} \delta(1-z) + \frac{\alpha_s(\mu)}{2\pi} \mathbb{K}_{ab}^{\overline{\text{MS}} \rightarrow \text{FS}}(z) + O(\alpha_s^2). \quad (\text{A.3})$$

The corresponding insertion operators for processes with two initial-state hadrons are given, for a colour-singlet final-state, by [33, eq. C.29]

$$P_{ab}(x, \mu) = -P_{ab}(x) \log \frac{\mu^2}{\hat{s}_{12}} \quad (\text{A.4})$$

where P_{ab} are the regularised DGLAP splitting kernels, and [33, eq. C.33]

$$K_{ab}(x, \mu) = \bar{K}_{ab}(x) + \tilde{K}_{ab}(x) - K_{ab}^{\text{FS}}(x), \quad (\text{A.5})$$

where full expressions for \bar{K}_{ab} and \tilde{K}_{ab} may be found in Appendix C of [33].

For colour-singlet processes, the relevant combinations of insertion operators simplify to

$$(\text{P}(\mu) + \text{K})_{qq}^{\text{FS}}(x) = C_{\text{F}} \left[4 \left[\frac{\log(1-x)}{1-x} \right]_+ - 2(1+x) \log(1-x) - \frac{1+x^2}{1-x} \log x \right. \\ \left. + 1-x + \left(\frac{2}{3} \pi^2 - 5 \right) \delta(1-x) - p_{qq}(x) \log \frac{\mu^2}{\hat{s}_{12}} - C_{\text{F}}^{-1} K_{qq}^{\text{FS}}(x) \right] \quad (\text{A.6})$$

$$(\text{P}(\mu) + \text{K})_{gq}^{\text{FS}}(x) = T_{\text{R}} \left[p_{gq}(x) \log \frac{(1-x)^2}{x} \right. \\ \left. + 2x(1-x) - p_{gq}(x) \log \frac{\mu^2}{\hat{s}_{12}} - T_{\text{R}}^{-1} K_{gq}^{\text{FS}}(x) \right], \quad (\text{A.7})$$

where the leading-order colour-factor-stripped regularised DGLAP splitting functions are given in four dimensions by

$$p_{qq}(x) = \left(\frac{1+x^2}{1-x} \right)_+ \equiv 2 \left(\frac{1}{1-x} \right)_+ - (1+x) + \frac{3}{2} \delta(1-x) \quad (\text{A.8})$$

$$p_{qg}(x) = \frac{1+(1-x)^2}{x} \quad (\text{A.9})$$

$$p_{gq}(x) = x^2 + (1-x)^2 \quad (\text{A.10})$$

$$p_{gg}(x) = 2 \left[\left(\frac{1}{1-x} \right)_+ + \frac{1-x}{x} - 1 + x(1-x) \right] + \frac{b_0}{C_{\text{A}}} \delta(1-x), \quad (\text{A.11})$$

and

$$b_0 = \frac{11}{6} C_{\text{A}} - \frac{2}{3} n_f T_{\text{R}}. \quad (\text{A.12})$$

The factorisation-scheme-dependent contributions $K_{ab}^{\text{FS}}(x)$, which are also the transition kernels of eq. (A.3) (transposed¹⁸) then allow us to write the insertion operators in any factorisation scheme in terms of the $\overline{\text{MS}}$ operators and the transition kernel,

$$(\text{P}(\mu) + \text{K})_{aq}^{\text{FS}}(x) = (\text{P}(\mu) + \text{K})_{aq}^{\overline{\text{MS}}}(x) - \text{K}_{qa}^{\overline{\text{MS}} \rightarrow \text{FS}}(x). \quad (\text{A.13})$$

The factorisation scheme kernels are, by definition,

$$\text{K}_{ab}^{\overline{\text{MS}} \rightarrow \overline{\text{MS}}}(x) \equiv 0 \equiv K_{ba}^{\overline{\text{MS}}}(x) \quad (\text{A.14})$$

for the $\overline{\text{MS}}$ scheme and

$$\text{K}_{qq}^{\overline{\text{MS}} \rightarrow \text{DIS}}(x) \equiv K_{qq}^{\text{DIS}}(x) = C_{\text{F}} \left[\frac{1+x^2}{1-x} \left(\log \frac{1-x}{x} - \frac{3}{4} \right) + \frac{1}{4} (5x+9) \right]_+ \quad (\text{A.15})$$

$$\text{K}_{gq}^{\overline{\text{MS}} \rightarrow \text{DIS}}(x) \equiv K_{gq}^{\text{DIS}}(x) = T_{\text{R}} \left[p_{gq}(x) \log \frac{1-x}{x} + 8x(1-x) - 1 \right] \quad (\text{A.16})$$

$$\text{K}_{gq}^{\overline{\text{MS}} \rightarrow \text{DIS}}(x) \equiv K_{gq}^{\text{DIS}}(x) = -\text{K}_{qq}^{\overline{\text{MS}} \rightarrow \text{DIS}} \quad (\text{A.17})$$

$$\text{K}_{gg}^{\overline{\text{MS}} \rightarrow \text{DIS}}(x) \equiv K_{gg}^{\text{DIS}}(x) = -2n_f \text{K}_{gq}^{\overline{\text{MS}} \rightarrow \text{DIS}} \quad (\text{A.18})$$

¹⁸The transposed indices arise from the difference between indexing the kernels for matrix-multiplication on a column vector of PDFs as in eqs. (A.1) and (A.2) and on a matrix of partonic cross-sections as in [33]. The same considerations apply to the splitting kernels.

for the DIS scheme¹⁹ [93]. In the Krk scheme, following from eqs. (2.56), (2.57), (A.6) and (A.7),

$$K_{qq}^{\overline{\text{MS}} \rightarrow \text{Krk}}(x) \equiv K_{qq}^{\text{Krk}}(x) = C_F \left[\left[\frac{1+x^2}{1-x} \log \frac{(1-x)^2}{x} + 1-x \right]_+ - \frac{3}{2} \delta(1-x) \right] \quad (\text{A.19})$$

$$= C_F \left[4 \left[\frac{\log(1-x)}{1-x} \right]_+ - 2(1+x) \log(1-x) - \frac{1+x^2}{1-x} \log x \right. \\ \left. + 1-x - \left(\frac{\pi^2}{3} + \frac{17}{4} \right) \delta(1-x) \right]$$

$$K_{gg}^{\overline{\text{MS}} \rightarrow \text{Krk}}(x) \equiv K_{gg}^{\text{Krk}}(x) = T_R \left[2p_{gq}(x) \log(1-x) - p_{gq}(x) \log x - p_{gq}(x) + 1 \right] \quad (\text{A.20})$$

and so

$$(\text{P}(\mu) + \text{K})_{qq}^{\text{Krk}}(x) = \text{P}_{qq}(x, \mu) + K_{qq}^{\overline{\text{MS}}}(x) - K_{qq}^{\overline{\text{MS}} \rightarrow \text{Krk}}(x) \quad (\text{A.21})$$

$$= -C_F p_{qq}(x) \log \frac{\mu^2}{\hat{s}_{12}} + \frac{1}{2} \Delta_0^{\text{Krk}} \delta(1-x) \quad (\text{A.22})$$

$$(\text{P}(\mu) + \text{K})_{gq}^{\text{Krk}}(x) = \text{P}_{gq}(x, \mu) + K_{gq}^{\overline{\text{MS}}}(x) - K_{gq}^{\overline{\text{MS}} \rightarrow \text{Krk}}(x) \quad (\text{A.23})$$

$$= -T_R p_{gq}(x) \log \frac{\mu^2}{\hat{s}_{12}}, \quad (\text{A.24})$$

again illustrating the justified exclusion of explicit collinear terms from the perturbative cross-section, with

$$\Delta_0^{\text{Krk}} = C_F \left(2\pi^2 - \frac{3}{2} \right) \quad (\text{A.25})$$

following directly from the difference between eq. (A.6) and eq. (A.19).

B PDFs in the Krk factorisation scheme

Throughout we use the CT18NLO PDF [74], transformed from the $\overline{\text{MS}}$ to the Krk factorisation scheme with the C++ code used for [30]. This interfaces with the LHAPDF 6 [97] library to perform the required convolution integrals on the interpolated PDF objects, writing the transformed PDFs as LHAPDF grids with the same (x, Q^2) knots as the original input PDF grid. CT18NLO PDFs in the $\overline{\text{MS}}$ and Krk schemes at 3 and 100 GeV are shown in fig. 8.

The transformation kernels for the Krk scheme for the quark and antiquark PDFs, $K_{qa}^{\overline{\text{MS}} \rightarrow \text{Krk}}$, are determined by the Catani–Seymour dipoles as outlined in appendix A. The Krk ‘DY’ scheme [28, 30] transforms only the quark PDFs and would be equally suitable for the processes considered in this paper. We use the ‘full’ Krk scheme which also transforms the gluon PDF as outlined in [29, 30].

¹⁹By convention, in the DIS scheme $K_{qq}^{\overline{\text{MS}} \rightarrow \text{DIS}}$ and $K_{gg}^{\overline{\text{MS}} \rightarrow \text{DIS}}$ are fixed by the requirement that the DIS PDFs satisfy momentum conservation locally in x -space (equivalently, by extending the constraint on the second Mellin moment implied by momentum conservation to all Mellin moments) [93–96].

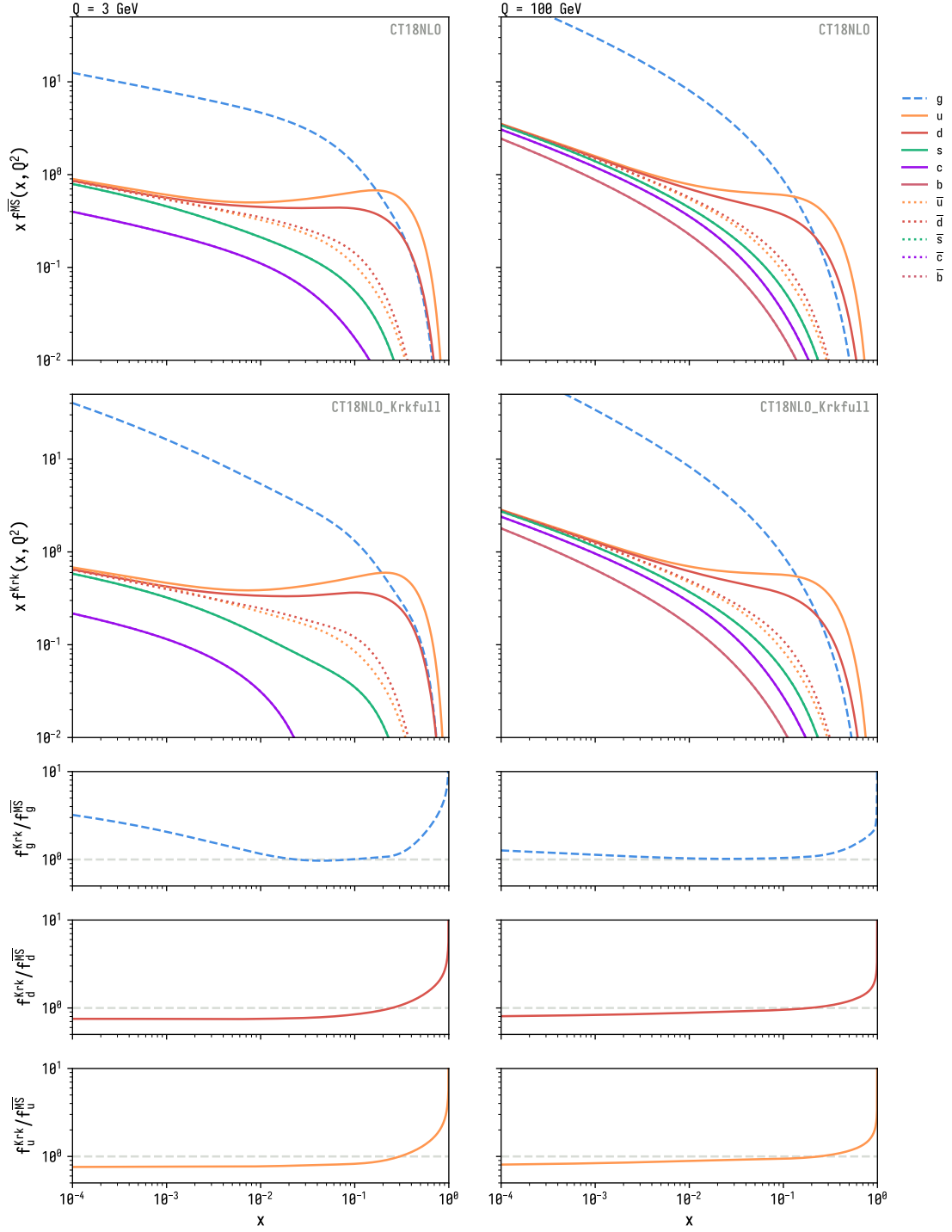


Figure 8: Comparison of the central CT18NLO [74] PDF set in the default $\overline{\text{MS}}$ factorisation scheme against the same PDF set transformed into the (full) Krk scheme as described in section 2.3 and appendix B. Left: $Q = 3$ GeV (for CT18NLO, $Q_0 = 1.3$ GeV); right: $Q = 100$ GeV.

Concretely, after imposing the momentum sum rule of eq. (2.58) [53], the transformation from the $\overline{\text{MS}}$ into the (full) Krk scheme is given by:

$$f_q^{\text{Krk}}(x, \mu_F) = f_q^{\overline{\text{MS}}}(x, \mu_F) \tag{B.1}$$

$$\begin{aligned} & - \frac{\alpha_s(\mu_F)}{2\pi} \frac{3}{2} C_F f_q^{\overline{\text{MS}}}(x, \mu_F) \\ & + \frac{\alpha_s(\mu_F)}{2\pi} C_F \int_x^1 \frac{dz}{z} \left[\frac{1+z^2}{1-z} \log \frac{(1-z)^2}{z} + 1-z \right]_+ f_q^{\overline{\text{MS}}}\left(\frac{x}{z}, \mu_F\right) \\ & + \frac{\alpha_s(\mu_F)}{2\pi} T_R \int_x^1 \frac{dz}{z} \left[p_{qq}(z) \log \frac{(1-z)^2}{z} + 2z(1-z) \right] f_g^{\overline{\text{MS}}}\left(\frac{x}{z}, \mu_F\right) \end{aligned}$$

$$f_g^{\text{Krk}}(x, \mu_F) = f_g^{\overline{\text{MS}}}(x, \mu_F) \tag{B.2}$$

$$\begin{aligned} & - \frac{\alpha_s(\mu_F)}{2\pi} C_A \left[\frac{\pi^2}{3} + \frac{341}{72} - \frac{59}{36} \frac{n_f T_R}{C_A} \right] f_g^{\overline{\text{MS}}}(x, \mu_F) \\ & + \frac{\alpha_s(\mu_F)}{2\pi} C_A \int_x^1 \frac{dz}{z} \left[4 \left[\frac{\log(1-x)}{1-x} \right]_+ - 2 \frac{\log z}{1-z} \right. \\ & \quad \left. + 2 \left(\frac{1}{z} - 2 + z(1-z) \right) \log \frac{(1-z)^2}{z} \right] f_g^{\overline{\text{MS}}}\left(\frac{x}{z}, \mu_F\right) \\ & + \frac{\alpha_s(\mu_F)}{2\pi} C_F \sum_{q_f, \bar{q}_f} \int_x^1 \frac{dz}{z} \left[p_{qg}(z) \log \frac{(1-z)^2}{z} + z \right] f_q^{\overline{\text{MS}}}\left(\frac{x}{z}, \mu_F\right) \end{aligned}$$

In the **C++** implementation the number of active light quark flavours in the above transformations is fixed at $n_f = 5$ for all scales μ , corresponding to using the fixed-flavour-number scheme (FFNS) for the transformation kernels.

C Validation

In this section we summarise the validation of the implementation of both the diphoton process within the KrkNLO code, and of the KrkNLO method more generally.

Real corrections

As described in section 3.2.1, it is possible to choose settings within KrkNLO which cause the KrkNLO implementation to calculate the fixed-order distribution, rather than the matched calculation. This is done by truncating the **Herwig** dipole shower to generate a single emission and reweighting by the reciprocal of the Sudakov factor, $1/\Delta|_{p_{T,1}}^{Q(\Phi_m)}(\Phi_m)$, as calculated numerically by integrating the competing shower emission kernels over their respective phase-spaces. We veto the no-emission events.

We perform the validation for the fiducial cuts of eq. (4.1), with the addition of a jet cut

$$p_T^j > 1 \text{ GeV}, \quad |\eta^j| < 5 \tag{C.1}$$

and with the generator cuts of eq. (4.2). Note that identified ‘jets’ at this order consist of exactly one parton.

The resulting distributions are shown in fig. 9 and show excellent agreement between the KrkNLO code and the **Matchbox** calculation of diphoton-plus-jet at leading order. This is a non-trivial test of the real weight eq. (2.49) and of the consistency of the Sudakov integration and unweighting with the shower algorithm.

Virtual corrections

As described in section 3.2.2, the virtual matrix elements within the KrkNLO implementation can be tested by setting the shower cut-off t_0 to ensure $t_0 > \max_{\Phi_m} Q(\Phi_m)$, prohibiting any parton-shower radiation. The shower algorithm is then bypassed and the Sudakov factor identically equal to 1 for all events. The components contributing to $\mathcal{O}(\Phi_m)$ in eq. (2.47) can then be tested numerically at the level of differential cross-sections against reference distributions calculated using the automated Matchbox implementation within Herwig, as shown in fig. 10.

Krk factorisation scheme

The PDF scheme transformation outlined in section 2.3 and appendix B and its compensating terms outlined in section 2.2 and appendix A ensure perturbative accuracy to NLO. Numerically, however, the reorganisation of the convolution between the hard process and the PDF is not guaranteed to give a numerically-identical result.

We test this explicitly in fig. 11 where we compare the Matchbox implementation of the Catani–Seymour P and K collinear counterterms to their KrkNLO counterparts, where the convolution is performed upon the PDFs to transform them into the Krk scheme and partially compensated by the Δ_0^{Krk} reweighting of the hard-process (concretely, the left- and right-hand sides of eq. (3.2)).

This is shown in fig. 11 and illustrates that the higher-order terms introduced to this contribution by the reorganisation of the convolution are approximately 5–10% of the total, varying primarily according to the rapidity-separation of the photon pair. This difference should be regarded as a contribution to the overall ‘missing-higher-order’ perturbative uncertainty.

References

- [1] S. Frixione and B.R. Webber, *Matching NLO QCD computations and parton shower simulations*, *JHEP* **06** (2002) 029 [[hep-ph/0204244](#)].
- [2] P. Nason, *A New method for combining NLO QCD with shower Monte Carlo algorithms*, *JHEP* **11** (2004) 040 [[hep-ph/0409146](#)].
- [3] S. Frixione, P. Nason and C. Oleari, *Matching NLO QCD computations with Parton Shower simulations: the POWHEG method*, *JHEP* **11** (2007) 070 [[0709.2092](#)].
- [4] S. Alioli, P. Nason, C. Oleari and E. Re, *A general framework for implementing NLO calculations in shower Monte Carlo programs: the POWHEG BOX*, *JHEP* **06** (2010) 043 [[1002.2581](#)].
- [5] S. Alioli, P. Nason, C. Oleari and E. Re, *NLO vector-boson production matched with shower in POWHEG*, *JHEP* **07** (2008) 060 [[0805.4802](#)].
- [6] S. Alioli, P. Nason, C. Oleari and E. Re, *NLO Higgs boson production via gluon fusion matched with shower in POWHEG*, *JHEP* **04** (2009) 002 [[0812.0578](#)].
- [7] S. Alioli, P. Nason, C. Oleari and E. Re, *NLO single-top production matched with shower in POWHEG: s- and t-channel contributions*, *JHEP* **09** (2009) 111 [[0907.4076](#)].
- [8] K. Hamilton, *A positive-weight next-to-leading order simulation of weak boson pair production*, *JHEP* **01** (2011) 009 [[1009.5391](#)].
- [9] S. Plätzer and S. Gieseke, *Dipole Showers and Automated NLO Matching in Herwig++*, *Eur. Phys. J. C* **72** (2012) 2187 [[1109.6256](#)].
- [10] S. Höche, F. Krauss, M. Schönherr and F. Siegert, *A critical appraisal of NLO+PS matching methods*, *JHEP* **09** (2012) 049 [[1111.1220](#)].
- [11] P. Nason and B. Webber, *Next-to-Leading-Order Event Generators*, *Ann. Rev. Nucl. Part. Sci.* **62** (2012) 187 [[1202.1251](#)].

- [12] R. Frederix, E. Re and P. Torrielli, *Single-top t -channel hadroproduction in the four-flavour scheme with POWHEG and aMC@NLO*, *JHEP* **09** (2012) 130 [[1207.5391](#)].
- [13] G. Heinrich, S.P. Jones, M. Kerner, G. Luisoni and E. Vryonidou, *NLO predictions for Higgs boson pair production with full top quark mass dependence matched to parton showers*, *JHEP* **08** (2017) 088 [[1703.09252](#)].
- [14] S. Jones and S. Kuttimalai, *Parton Shower and NLO-Matching uncertainties in Higgs Boson Pair Production*, *JHEP* **02** (2018) 176 [[1711.03319](#)].
- [15] K. Cormier, S. Plätzer, C. Reuschle, P. Richardson and S. Webster, *Parton showers and matching uncertainties in top quark pair production with Herwig 7*, *Eur. Phys. J. C* **79** (2019) 915 [[1810.06493](#)].
- [16] B. Jäger, A. Karlberg, S. Plätzer, J. Scheller and M. Zaro, *Parton-shower effects in Higgs production via Vector-Boson Fusion*, *Eur. Phys. J. C* **80** (2020) 756 [[2003.12435](#)].
- [17] ATLAS collaboration, *Studies on the improvement of the matching uncertainty definition in top-quark processes simulated with Powheg+Pythia 8*, Tech. Rep. [ATL-PHYS-PUB-2023-029](#), CERN, Geneva (2023).
- [18] K. Hamilton, P. Nason, E. Re and G. Zanderighi, *NNLOPS simulation of Higgs boson production*, *JHEP* **10** (2013) 222 [[1309.0017](#)].
- [19] S. Plätzer, *Controlling inclusive cross sections in parton shower + matrix element merging*, *JHEP* **08** (2013) 114 [[1211.5467](#)].
- [20] L. Lönnblad and S. Prestel, *Merging Multi-leg NLO Matrix Elements with Parton Showers*, *JHEP* **03** (2013) 166 [[1211.7278](#)].
- [21] S. Höche, Y. Li and S. Prestel, *Higgs-boson production through gluon fusion at NNLO QCD with parton showers*, *Phys. Rev. D* **90** (2014) 054011 [[1407.3773](#)].
- [22] J. Bellm, S. Gieseke and S. Plätzer, *Merging NLO Multi-jet Calculations with Improved Unitarization*, *Eur. Phys. J. C* **78** (2018) 244 [[1705.06700](#)].
- [23] S. Alioli, C.W. Bauer, C.J. Berggren, A. Hornig, F.J. Tackmann, C.K. Vermilion et al., *Combining Higher-Order Resummation with Multiple NLO Calculations and Parton Showers in GENEVA*, *JHEP* **09** (2013) 120 [[1211.7049](#)].
- [24] S. Alioli, C.W. Bauer, C. Berggren, F.J. Tackmann, J.R. Walsh and S. Zuberi, *Matching Fully Differential NNLO Calculations and Parton Showers*, *JHEP* **06** (2014) 089 [[1311.0286](#)].
- [25] S. Alioli, C.W. Bauer, C. Berggren, F.J. Tackmann and J.R. Walsh, *Drell-Yan production at NNLL'+NNLO matched to parton showers*, *Phys. Rev. D* **92** (2015) 094020 [[1508.01475](#)].
- [26] P.F. Monni, P. Nason, E. Re, M. Wiesemann and G. Zanderighi, *MiNNLO_{PS}: a new method to match NNLO QCD to parton showers*, *JHEP* **05** (2020) 143 [[1908.06987](#)].
- [27] S. Jadach, A. Kusina, W. Płaczek, M. Skrzypek and M. Sławska, *Inclusion of the QCD next-to-leading order corrections in the quark-gluon Monte Carlo shower*, *Phys. Rev. D* **87** (2013) 034029 [[1103.5015](#)].
- [28] S. Jadach, W. Płaczek, S. Sapeta, A. Siódmok and M. Skrzypek, *Matching NLO QCD with parton shower in Monte Carlo scheme — the KrkNLO method*, *JHEP* **10** (2015) 052 [[1503.06849](#)].
- [29] S. Jadach, G. Nail, W. Płaczek, S. Sapeta, A. Siódmok and M. Skrzypek, *Monte Carlo simulations of Higgs-boson production at the LHC with the KrkNLO method*, *Eur. Phys. J. C* **77** (2017) 164 [[1607.06799](#)].
- [30] S. Jadach, W. Płaczek, S. Sapeta, A. Siódmok and M. Skrzypek, *Parton distribution functions in Monte Carlo factorisation scheme*, *Eur. Phys. J. C* **76** (2016) 649 [[1606.00355](#)].

- [31] S. Jadach, M. Jeżabek, A. Kusina, W. Placzek and M. Skrzypek, *NLO corrections to hard process in QCD shower – proof of concept*, *Acta Phys. Polon. B* **43** (2012) 2067 [[1209.4291](#)].
- [32] S. Jadach, *On the universality of the KRK factorization scheme*, *Acta Phys. Polon. B* **51** (2020) 1363 [[2004.04239](#)].
- [33] S. Catani and M.H. Seymour, *A General algorithm for calculating jet cross-sections in NLO QCD*, *Nucl. Phys. B* **485** (1997) 291 [[hep-ph/9605323](#)].
- [34] M.H. Seymour, *Matrix element corrections to parton shower algorithms*, *Comput. Phys. Commun.* **90** (1995) 95 [[hep-ph/9410414](#)].
- [35] T. Sjöstrand, S. Mrenna and P.Z. Skands, *PYTHIA 6.4 Physics and Manual*, *JHEP* **05** (2006) 026 [[hep-ph/0603175](#)].
- [36] S. Plätzer and M. Sjö Dahl, *The Sudakov Veto Algorithm Reloaded*, *Eur. Phys. J. Plus* **127** (2012) 26 [[1108.6180](#)].
- [37] L. Lönnblad, *Fooling Around with the Sudakov Veto Algorithm*, *Eur. Phys. J. C* **73** (2013) 2350 [[1211.7204](#)].
- [38] R. Kleiss and R. Verheyen, *Competing Sudakov Veto Algorithms*, *Eur. Phys. J. C* **76** (2016) 359 [[1605.09246](#)].
- [39] Z. Nagy and D.E. Soper, *Matching parton showers to NLO computations*, *JHEP* **10** (2005) 024 [[hep-ph/0503053](#)].
- [40] Z. Nagy and D.E. Soper, *A New parton shower algorithm: Shower evolution, matching at leading and next-to-leading order level*, in *Ringberg Workshop on New Trends in HERA Physics 2005*, pp. 101–123, 1, 2006, DOI [[hep-ph/0601021](#)].
- [41] M. Dinsdale, M. Ternick and S. Weinzierl, *Parton showers from the dipole formalism*, *Phys. Rev. D* **76** (2007) 094003 [[0709.1026](#)].
- [42] S. Schumann and F. Krauss, *A Parton shower algorithm based on Catani-Seymour dipole factorisation*, *JHEP* **03** (2008) 038 [[0709.1027](#)].
- [43] S. Plätzer and S. Gieseke, *Coherent Parton Showers with Local Recoils*, *JHEP* **01** (2011) 024 [[0909.5593](#)].
- [44] J. Bellm et al., *Herwig 7.0/Herwig++ 3.0 release note*, *Eur. Phys. J. C* **76** (2016) 196 [[1512.01178](#)].
- [45] G. Bewick et al., *Herwig 7.3 release note*, *Eur. Phys. J. C* **84** (2024) 1053 [[2312.05175](#)].
- [46] S. Catani, S. Dittmaier, M.H. Seymour and Z. Trócsányi, *The Dipole formalism for next-to-leading order QCD calculations with massive partons*, *Nucl. Phys. B* **627** (2002) 189 [[hep-ph/0201036](#)].
- [47] S. Plätzer, *Parton Showers and Radiative Corrections in QCD*, Ph.D. thesis, Karlsruhe U., 2010.
- [48] T. Sjöstrand, *A Model for Initial State Parton Showers*, *Phys. Lett. B* **157** (1985) 321.
- [49] S. Plätzer, A. Siódmok and J. Whitehead, *Negative weight reduction for NLO matching with Matchbox*, in preparation (2024) .
- [50] HERWIG collaboration, *The Physics of Herwig 7*, in preparation (2024) .
- [51] T. Plehn, D. Rainwater and P.Z. Skands, *Squark and gluino production with jets*, *Phys. Lett. B* **645** (2007) 217 [[hep-ph/0510144](#)].
- [52] R. Corke and T. Sjöstrand, *Improved Parton Showers at Large Transverse Momenta*, *Eur. Phys. J. C* **69** (2010) 1 [[1003.2384](#)].
- [53] J.C. Collins and D.E. Soper, *Parton Distribution and Decay Functions*, *Nucl. Phys. B* **194** (1982) 445.
- [54] S. Gieseke, *Uncertainties of Sudakov form-factors*, *JHEP* **01** (2005) 058 [[hep-ph/0412342](#)].

- [55] J. Bellm, S. Plätzer, P. Richardson, A. Siódmok and S. Webster, *Reweighting Parton Showers*, *Phys. Rev. D* **94** (2016) 034028 [[1605.08256](#)].
- [56] E. Bothmann, M. Schönherr and S. Schumann, *Reweighting QCD matrix-element and parton-shower calculations*, *Eur. Phys. J. C* **76** (2016) 590 [[1606.08753](#)].
- [57] S. Mrenna and P. Skands, *Automated Parton-Shower Variations in Pythia 8*, *Phys. Rev. D* **94** (2016) 074005 [[1605.08352](#)].
- [58] J. Bellm, G. Nail, S. Plätzer, P. Schichtel and A. Siódmok, *Parton Shower Uncertainties with Herwig 7: Benchmarks at Leading Order*, *Eur. Phys. J. C* **76** (2016) 665 [[1605.01338](#)].
- [59] T. Gehrmann, E. Glover, A. Huss and J. Whitehead, *Scale and isolation sensitivity of diphoton distributions at the LHC*, *JHEP* **01** (2021) 108 [[2009.11310](#)].
- [60] S. Catani, B.R. Webber and G. Marchesini, *QCD coherent branching and semiinclusive processes at large x* , *Nucl. Phys. B* **349** (1991) 635.
- [61] J. Bellm et al., *Herwig 7.1 Release Note*, [1705.06919](#).
- [62] J. Bellm et al., *Herwig 7.2 release note*, *Eur. Phys. J. C* **80** (2020) 452 [[1912.06509](#)].
- [63] P. Nason and G.P. Salam, *Multiplicative-accumulative matching of NLO calculations with parton showers*, *JHEP* **01** (2022) 067 [[2111.03553](#)].
- [64] F. Buccioni, J.-N. Lang, J.M. Lindert, P. Maierhöfer, S. Pozzorini, H. Zhang et al., *OpenLoops 2*, *Eur. Phys. J. C* **79** (2019) 866 [[1907.13071](#)].
- [65] J. Alwall, R. Frederix, S. Frixione, V. Hirschi, F. Maltoni, O. Mattelaer et al., *The automated computation of tree-level and next-to-leading order differential cross sections, and their matching to parton shower simulations*, *JHEP* **07** (2014) 079 [[1405.0301](#)].
- [66] G.P. Lepage, *A New Algorithm for Adaptive Multidimensional Integration*, *J. Comput. Phys.* **27** (1978) 192.
- [67] P. Nason and G. Ridolfi, *A Positive-weight next-to-leading-order Monte Carlo for Z pair hadroproduction*, *JHEP* **08** (2006) 077 [[hep-ph/0606275](#)].
- [68] K. Hamilton, P. Richardson and J. Tully, *A Positive-Weight Next-to-Leading Order Monte Carlo Simulation of Drell-Yan Vector Boson Production*, *JHEP* **10** (2008) 015 [[0806.0290](#)].
- [69] F. Febres Cordero, M. Kraus and L. Reina, *Top-quark pair production in association with a W^\pm gauge boson in the POWHEG-BOX*, *Phys. Rev. D* **103** (2021) 094014 [[2101.11808](#)].
- [70] ATLAS collaboration, *Measurement of the production cross section of pairs of isolated photons in pp collisions at 13 TeV with the ATLAS detector*, *JHEP* **11** (2021) 169 [[2107.09330](#)].
- [71] S. Frixione, *Isolated photons in perturbative QCD*, *Phys. Lett. B* **429** (1998) 369 [[hep-ph/9801442](#)].
- [72] J.R. Andersen et al., *Les Houches 2013: Physics at TeV Colliders: Standard Model Working Group Report*, [1405.1067](#).
- [73] M. Cacciari, G.P. Salam and G. Soyez, *The anti- k_t jet clustering algorithm*, *JHEP* **04** (2008) 063 [[0802.1189](#)].
- [74] T.-J. Hou et al., *New CTEQ global analysis of quantum chromodynamics with high-precision data from the LHC*, *Phys. Rev. D* **103** (2021) 014013 [[1912.10053](#)].
- [75] C. Bierlich et al., *Robust Independent Validation of Experiment and Theory: Rivet version 3*, *SciPost Phys.* **8** (2020) 026 [[1912.05451](#)].
- [76] S. Catani, L. Cieri, D. de Florian, G. Ferrera and M. Grazzini, *Diphoton production at hadron colliders: a fully-differential QCD calculation at NNLO*, *Phys. Rev. Lett.* **108** (2012) 072001 [[1110.2375](#)].

- [77] J.M. Campbell, R.K. Ellis, Y. Li and C. Williams, *Predictions for diphoton production at the LHC through NNLO in QCD*, *JHEP* **07** (2016) 148 [[1603.02663](#)].
- [78] H.A. Chawdhry, M. Czakon, A. Mitov and R. Poncelet, *NNLO QCD corrections to diphoton production with an additional jet at the LHC*, *JHEP* **09** (2021) 093 [[2105.06940](#)].
- [79] A. Gavardi, C. Oleari and E. Re, *NNLO+PS Monte Carlo simulation of photon pair production with MiNNLO_{PS}*, *JHEP* **09** (2022) 061 [[2204.12602](#)].
- [80] S. Höche, F. Krauss, M. Schönherr and F. Siegert, *QCD matrix elements + parton showers: The NLO case*, *JHEP* **04** (2013) 027 [[1207.5030](#)].
- [81] GoSAM collaboration, *Automated One-Loop Calculations with GoSam*, *Eur. Phys. J. C* **72** (2012) 1889 [[1111.2034](#)].
- [82] GoSAM collaboration, *GOSAM-2.0: a tool for automated one-loop calculations within the Standard Model and beyond*, *Eur. Phys. J. C* **74** (2014) 3001 [[1404.7096](#)].
- [83] S. Höche and M. Schönherr, *Uncertainties in next-to-leading order plus parton shower matched simulations of inclusive jet and dijet production*, *Phys. Rev. D* **86** (2012) 094042 [[1208.2815](#)].
- [84] S. Dittmaier et al., *Handbook of LHC Higgs Cross Sections: 2. Differential Distributions*, [1201.3084](#).
- [85] R.V. Harlander, H. Mantler and M. Wiesemann, *Transverse momentum resummation for Higgs production via gluon fusion in the MSSM*, *JHEP* **11** (2014) 116 [[1409.0531](#)].
- [86] E. Bagnaschi and A. Vicini, *The Higgs transverse momentum distribution in gluon fusion as a multiscale problem*, *JHEP* **01** (2016) 056 [[1505.00735](#)].
- [87] E. Bagnaschi, R.V. Harlander, H. Mantler, A. Vicini and M. Wiesemann, *Resummation ambiguities in the Higgs transverse-momentum spectrum in the Standard Model and beyond*, *JHEP* **01** (2016) 090 [[1510.08850](#)].
- [88] R. Frederix, S. Frixione, S. Prestel and P. Torrielli, *On the reduction of negative weights in MC@NLO-type matching procedures*, *JHEP* **07** (2020) 238 [[2002.12716](#)].
- [89] P. Nason and C. Oleari, *NLO Higgs boson production via vector-boson fusion matched with shower in POWHEG*, *JHEP* **02** (2010) 037 [[0911.5299](#)].
- [90] A. Banfi, S. Ferrario Ravasio, B. Jäger, A. Karlberg, F. Reichenbach and G. Zanderighi, *A POWHEG generator for deep inelastic scattering*, *JHEP* **02** (2024) 023 [[2309.02127](#)].
- [91] ATLAS collaboration, *Comparison of Monte Carlo generator predictions to ATLAS measurements of top pair production at 7 TeV*, Tech. Rep. ATL-PHYS-PUB-2015-002 (2015).
- [92] ATLAS collaboration, *Studies of $t\bar{t}/tW$ interference effects in $b\bar{b}\ell^+\ell'^-\nu\bar{\nu}'$ final states with Powheg and MG5_aMC@NLO setups*, Tech. Rep. ATL-PHYS-PUB-2021-042 (2021).
- [93] G. Altarelli, R.K. Ellis and G. Martinelli, *Large Perturbative Corrections to the Drell-Yan Process in QCD*, *Nucl. Phys. B* **157** (1979) 461.
- [94] M. Diemoz, F. Ferroni, E. Longo and G. Martinelli, *Parton Densities from Deep Inelastic Scattering to Hadronic Processes at Super Collider Energies*, *Z. Phys. C* **39** (1988) 21.
- [95] S. Catani and F. Hautmann, *High-energy factorization and small x deep inelastic scattering beyond leading order*, *Nucl. Phys. B* **427** (1994) 475 [[hep-ph/9405388](#)].
- [96] A.D. Martin, R.G. Roberts, W.J. Stirling and R.S. Thorne, *Scheme dependence, leading order and higher twist studies of MRST partons*, *Phys. Lett. B* **443** (1998) 301 [[hep-ph/9808371](#)].
- [97] A. Buckley, J. Ferrando, S. Lloyd, K. Nordström, B. Page, M. Rüfenacht et al., *LHAPDF6: parton density access in the LHC precision era*, *Eur. Phys. J. C* **75** (2015) 132 [[1412.7420](#)].

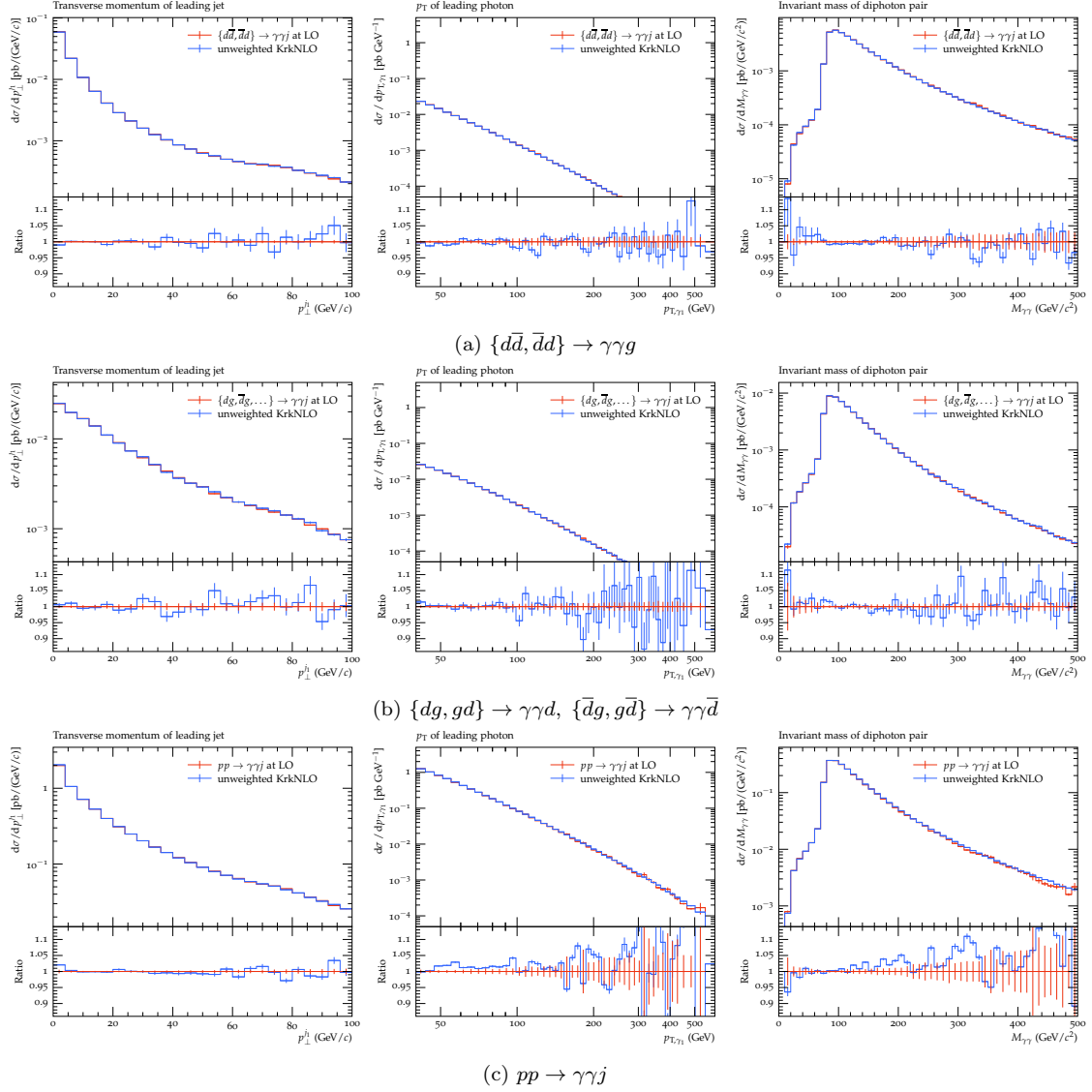


Figure 9: Validation of the real weight for the $q\bar{q}$ -, qg - and pp -channels respectively by unweighting by the Sudakov factor $\Delta|_{p_{T,1}}^{Q(\Phi_m)}(\Phi_m)$ (independently calculated for each emission by numerical integration of the kernels over the radiative phase-space) to isolate the real matrix element within the KrkNLO implementation, as described in section 3.2.1.

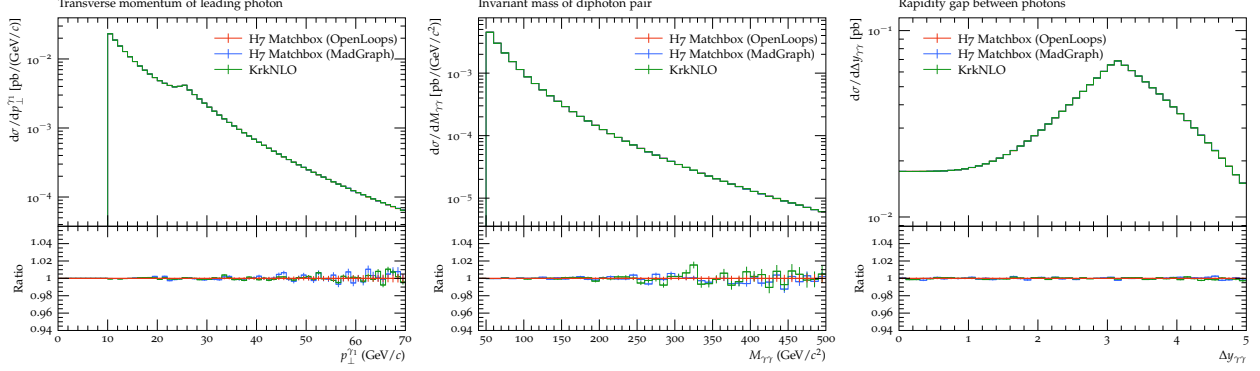


Figure 10: Validation of the virtual weight $V + I$ for the $q\bar{q}$ -channel as described in section 3.2.2. By setting the shower IR cutoff to guarantee $t_0 > Q(\Phi_m)$, thus disabling the shower, and manually disabling the Born and Δ_0^{FS} contributions within KrkNLO, the KrkNLO implementation of the virtual terms can be compared with those generated automatically by Matchbox within Herwig 7.

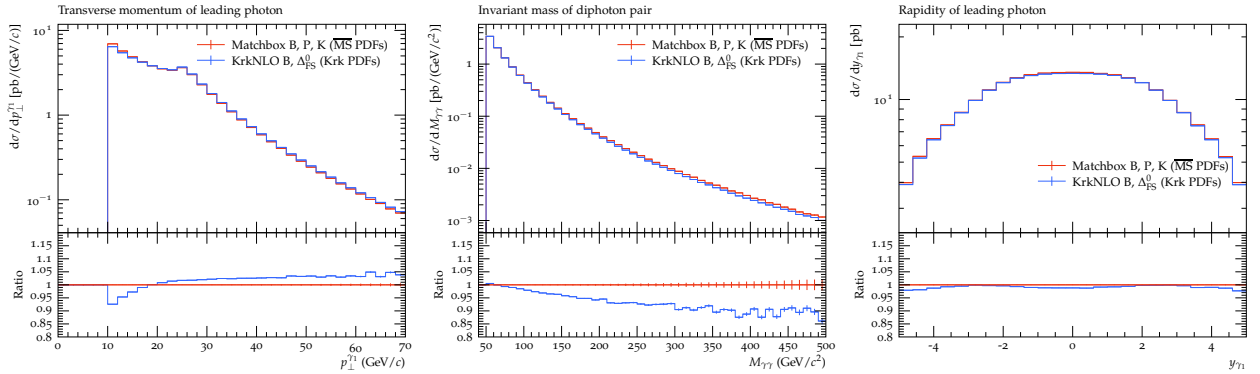


Figure 11: Validation of the Krk PDF scheme transformation and associated Δ_0^{FS} correction as described in section 3.2.3. Plots shown for $pp \rightarrow \gamma\gamma$ at $\sqrt{s} = 8 \text{ TeV}$, for running α_s with $\alpha_s(M_Z) = 0.118$ and the CT18NLO PDF set.